AD717082

GEORGIA INSTITUTE OF TECHNOLOGY
Engineering Experiment Station
Atlanta, Georgia

Final Technical Report
Project A-1268

LOW-ANGLE RADAR SEA RETURN AT 3-mm WAVELENGTH

by

Wayne Rivers

Contract No. N62269-70-C-0489

15 November 1970

Prepared for
Department of the Navy
Naval Air Development Center
Johnsville, Pennsylvania 18974

84

GEORGIA INSTITUTE OF TECHNOLOGY
Engineering Experiment Station
Atlanta, Georgia

Final Technical Report
Project A-1268

LOW-ANGLE RADAR SEA RETURN AT 3-mm WAVELENGTH

by

Wayne Rivers

Contract No. N62269-70-C-0489

15 November 1970

Prepared for
Department of the Navy
Naval Air Development Center
Johnsville, Pennsylvania 18974

TABLE OF CONTENTS

TABLE OF CONTENTS (Cont.)

LIST OF FIGURES

LIST OF FIGURES (Continued)

LIST OF TABLES

LOW-ANGLE RADAR SEA RETURN AT 3-mm WAVELENGTH

by

Wayne Rivers

ABSTRACT

Measurements of radar return from the sea and targets on the sea have been made at incidence angles near grazing with a 3-millimeter radar developed and operated by personnel of the Naval Air Development Center, Johnsville, Pa. The results show similarities in many respects to sea return at longer wavelengths, but they are strikingly different in a few instances. Notable are that the trend for cross section per unit area to increase with decreasing wavelength from 10 to 3 cm is not continued between 3 cm and 3 mm, and that the return for vertical polarization is substantially less than that for horizontal polarization for all conditions observed. Also included in the study are indications of angle, wind-speed, and boresight-wind-vector angle dependences of sea return.

I. INTRODUCTION

A. History

Radar sea return can be characterized as a randomly varying signal with statistics which are deterministic functions of radar, geometric and environmental variables. Not all of these variables are known, and, for those that have been studied extensively for thirty or so years, the deterministic functions are not yet defined with precision, although many are clear enough to be useful for some scientific and engineering purposes. Research on the nature of radar sea clutter has for the most part been led by experiment rather than by theory, and this investigation follows that pattern. Data will be presented and discussed from a series of observations designed to establish some of the properties of sea clutter at a radar wavelength of 3 mm, where heretofore no data and only poor quality theory and extrapolation of experimental trends have been available.

Outstanding among the statistics which can be used to describe radar sea clutter signals is the "average cross-section per unit area," denoted by the symbol $\sigma°$. The value of this statistic was pointed out by Herbert Goldstein [1], and lies in the fact that estimates of it by different observers with unique radars should agree under the same geometric and environmental conditions. For the low-grazing-angle pulsed-radar case, in which the radar cell is defined by the pulse shape in range and the azimuth beam shape of the antenna in the transverse direction, $\sigma°$ is defined by

$$\sigma° = \frac{\int \sigma(\xi,\eta)\, W_r(\xi)\, W_a(\eta)\, d\xi d\eta}{\int W_r(\xi)\, W_a(\eta)\, d\xi d\eta}, \tag{1}$$

in which $\sigma(\xi,\eta)d\xi d\eta$ is the intrinsic microscopic cross section of a patch of sea surface defined by area $d\xi d\eta$ at coordinates ξ and η, and W_r and W_a are power response weighting functions in the range and azimuth directions, respectively, which define the shape of the cell. The average is conventionally taken over time, with all other variables of the problem held fixed, implicitly.

One of the most striking dependences of $\sigma°$ already observed at long wavelengths is on the incidence angle,* denoted herein by ψ. The angle function is easily divided into three angle regions. The "high-angle" region near $\psi = 90$ degrees, or vertical, is marked by a rapid decrease of $\sigma°$ with decreasing angle. Adjacent is the "plateau" region where the angle dependence is weak, about like $\psi^{0.4}$. Near grazing, the "low-angle" region exhibits a rapid fall-off of $\sigma°$ with decreasing angle, which is associated with interference between direct and surface-reflected rays. The interference effect is strongly frequency sensitive, so that both the location of the transition angle dividing the plateau and low-angle regions, and the value of $\sigma°$ in the low-angle region are dependent on wavelength, the latter strongly so. Thus, it is especially difficult to compare data across wavelengths and to extrapolate levels to new frequency bands when near-grazing angles are involved. Even when the low-angle region is avoided, many wavelength effects are active, and it is this author's contention that an adequate experiment to determine the wavelength dependences of sea return has not yet been carried out. The angle region accessible in the present experiment was such that some low-angle effects are clearly visible in the 3.2-cm radar data which were used as controls for the 3-mm radar data.

A consensus of available data [2] obtained at longer wavelengths (30 to 0.8 cm) and applicable to the plateau region shows a monotonic increase of $\sigma°$ with frequency for a given sea state. This trend is confirmed by one of the two outstanding multifrequency experiments involving the millimeter region [3] but the other exhibits an opposite trend [4].

Other dependences which have been studied are sea state (specified by wind speed and wave height at least), angle between radar boresight and wind vector, and polarization. Increasing sea state results in

*In this report the emphasis is on near-horizontal propagation, so the angle is chosen to be zero for horizontal and 90 degrees for vertical incidence.

monotonic increase in $\sigma°$ at microwave frequencies. Higher values of $\sigma°$ are seen looking upwind (or sometimes "up-wave") than in other directions, and at lower frequencies average return for vertical polarization is substantially greater than for horizontal at low sea states. At high sea states, return on vertical may be slightly lower than horizontal (perhaps by 2 dB), especially at X-band and higher frequencies and at the lower grazing angles.

The experiments described herein were performed during the period 27 July 1970 through 21 August 1970. Data acquisition was begun on 30 July and terminated on 19 August. The observations were made with existing radars and instrumentation so that physical preparations required for the experiments were minimal. A weatherproof enclosure for the 3-mm radar was constructed and installed on the tower supporting the existing experimental X-band radar during the week of 13 July. On 16 days of the active period 494 data runs of all types were recorded of which 263 (53%) were for calibration purposes; of the remainder, 172 were on sea return and 59 on targets on the sea. Approximately 76% of the data were taken with the NADC 3-mm radar and 24% at X-band. Of the clutter and target runs it was found that 196, or 85%, could be adequately calibrated and used for further analysis. These partially reduced data are included in Appendix B of this report.

The following variables and the available range of their changes were studied:

Wavelength (frequency)	3 mm and 3.2 cm (95 and 9.4 GHz)
Radar range*	1.7 to 12.4 μs
Incidence angle	5 to 0.7 degree
Wind speed	2 to 14 knots
Wave height (av.)	0.5 to 2.5 feet
Polarization	VV and HH
Upwind-boresight aspect angle	Upwind around to crosswind

Because weather conditions which control variability of the data do change with time, the data runs were structured so as to change one variable at a

*Range in this report is expressed as 2-way time of flight. Thus, 1 μs ≈ 150 m.

time, holding all others fixed if possible. In this way, some of the "on-diagonal" trends or functional dependences of σ° on the above variables could be displayed. It is known from lower-frequency data that the functions of some of the variables interact strongly with other variables, but unfortunately there was insufficient time in this experiment to establish these "off-diagonal" joint functions to any significant degree.

B. Report Organization

This report is structured in the following way. The instrumentation and manner in which the data were obtained and processed are described in Chapter II and supported with the material in Appendix A. The totality of useful cross section data, which was the principal result from the observations, is assembled in Appendix B. From these data, subsets are extracted and analyzed in Chapters III and IV for sea return and targets on the sea, respectively. The results in those chapters are presented largely without interpretation which is given separately in Chapter V.

C. Summary

The return from targets on the sea and sea clutter have been measured with 3-mm radar at a shore site. The sea-return measurements show trends with changes in geometry and environment variables which are similar to those generally observed at low frequencies. The average cross section per unit area, σ°, increases with increasing wind speed and is generally larger for upwind return than for crosswind look directions. The dependence on wind speed, W, is approximately $\sigma^\circ \propto W^{1.5}$ at an incidence angle of 1.4 degrees and $\sigma^\circ \propto W^4$ at 2.8 degrees. Only low and moderate wind conditions were experienced, so it is not known if saturation of σ° occurs for high sea states. The angle dependence near grazing is between ψ^0 and ψ^{+1} for rough water and upwind look direction, but it can be inversely proportional to angle for low-sea or crosswind look directions. Contradictory to most low-frequency experience is that σ°_{HH} is greater than σ°_{VV} by about 5 dB, average. This is attributed to increased transparency of the water for vertical polarization at near-grazing incidence caused by the relatively low dielectric constant of water at high frequencies. Comparison of σ° values measured at 3 mm with those measured at X-band and reported elsewhere indicates that σ° does not increase with frequency much above X-band,

and that at the higher sea states some decrease is evident. The statistical distributions of sea return signals are similar to those for lower frequencies and have shapes that are approximately log-normal. Typically the widths for horizontal polarization are greater than for vertical, and standard deviations are near 7 and 4.7 dB, respectively. Autocorrelation functions of 3-mm sea return resemble those of X-band clutter signals, except that the Doppler decorrelation time is less because of the higher radar frequency. The sea-surface gross-structure effects on the autocorrelation function are undistorted by the change in frequency.

Effective cross sections of targets on the sea were measured. Values for boats ranged from -6 to 0 dBsm for small craft, and from 0 to +16 dBsm for larger ones. Values for sonobuoys averaged -10 dBsm but ranged from -20 to 0 dBsm depending on sea conditions and incidence angle (range). The effect of shadowing of small targets by wave crests was evident at longer ranges and higher sea states, resulting in lower average cross sections and bimodal amplitude distributions.

II. INSTRUMENTATION AND TECHNIQUE

A. Radar Parameters and Descriptions

The experimental data were obtained at a coastal site near Boca Raton, Florida. The tower supporting the radars is located on the berne approximately 125 feet from the water's edge. Location of the site is shown in Figure 1 and a profile of the sea bottom east of the site is shown in Figure 2. The instrumentation was enclosed in a van at the base of the tower. A photograph of the tower and support buildings taken from southwest of the tower is shown in Figure 3. Pertinent details of the radars follow.

1. The 3-mm radar. The millimeter radar was constructed by personnel of the Naval Air Development Center and operated by them during this experiment. Parameters applicable to this experiment are listed in Table I along with others of peripheral interest. The entire radar was placed in a small hut on the seaward side of the tower at a level so that the antenna was 75 feet above the water. A permanent radome of 0.005 inch Mylar was installed across the front of the hut to protect the system. Evaluation of the effect of the radome was limited to observing antenna sidelobe levels, which were more than 40 dB below the beam peak, 2-way. In any case, both observations and calibration were performed through the radome, so that its loss should not affect the measurements.

The radar was calibrated by observing the return from a trihedral corner reflector mounted 15 feet above a piling bearing 92 degrees magnetic at a range of 2240 feet from the radar. The corner had an interior edge dimension of 2.813 $\pm$ 0.015 inch, which is dimension, a, of the cross-section formula [5]

$$\sigma_s = \frac{4}{3} \pi \frac{a^4}{\lambda^2} . \tag{2}$$

Using a nominal wavelength of 0.124 inch (corresponding to 3.16 mm and a frequency of 95 GHz), a cross section of 118.5 ft^2 or 11 m^2 is calculated (corresponding to +10.4 dBsm). A calibrated attenuator (TRG E-510-31) was included in the receiver input and was used to reference return levels from the corner to those from targets under measurement. Additional discussion of the measurement technique is included in Section C of this chapter.

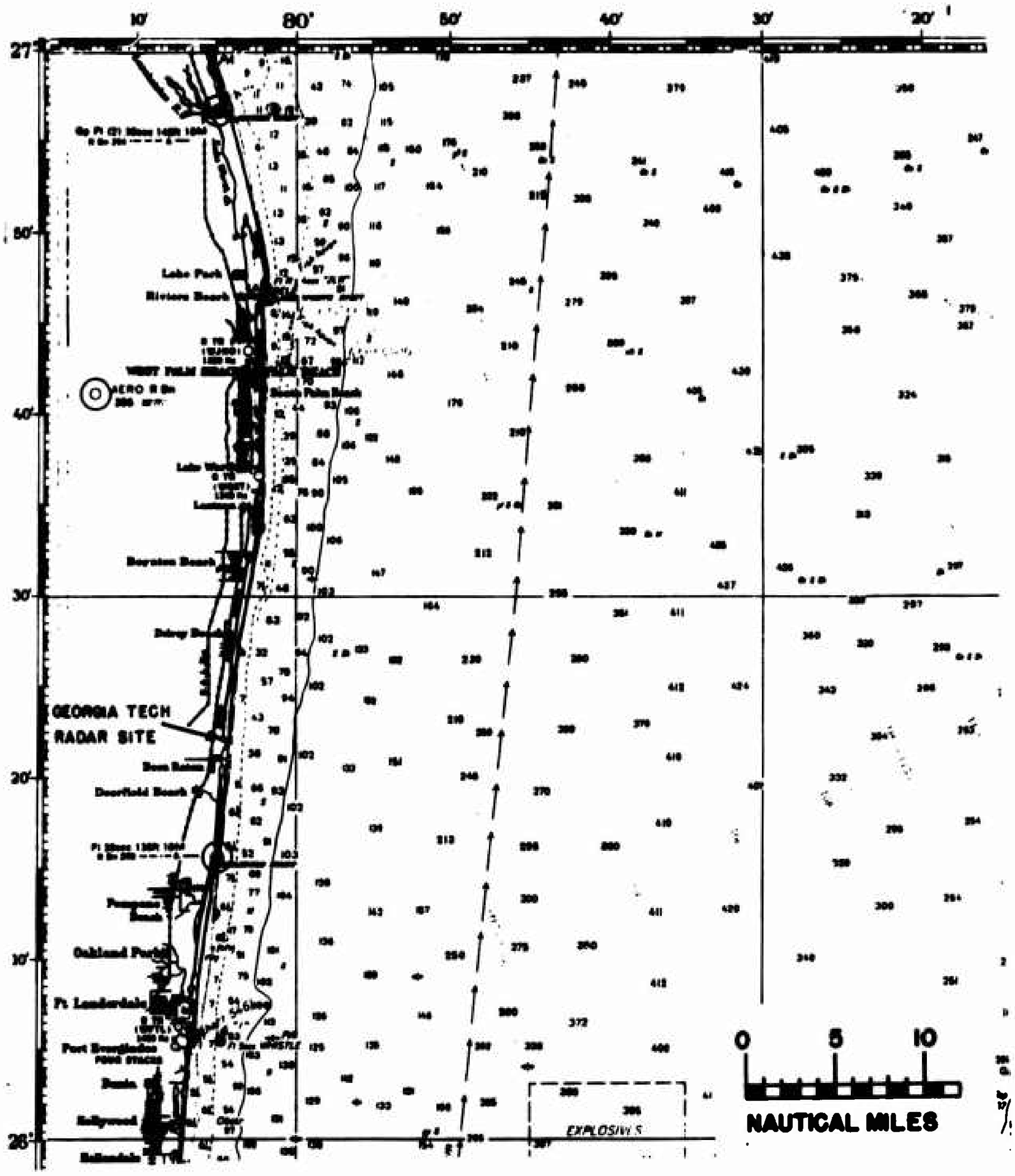

Figure 1. Chart of Boca Raton Field Site.

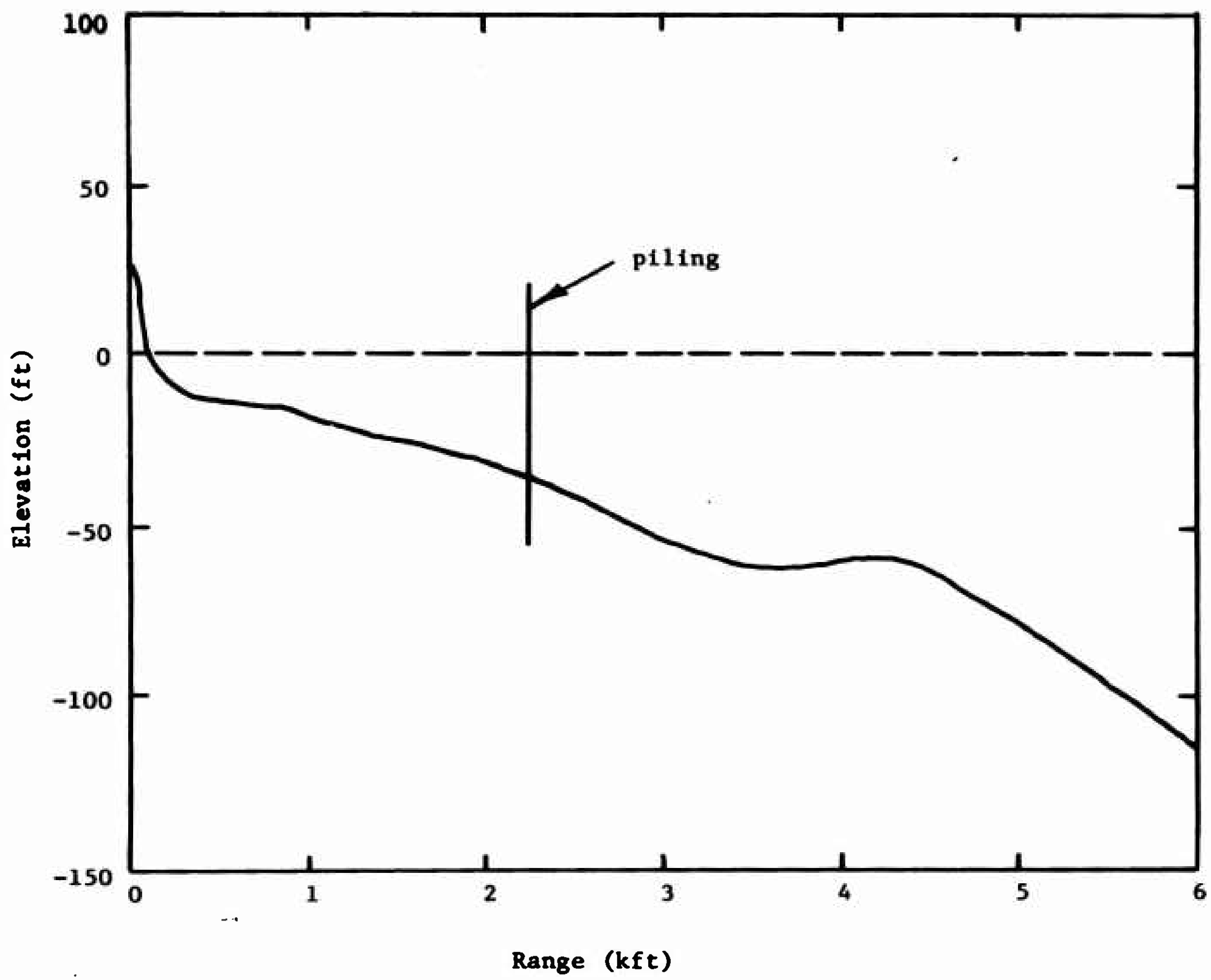

Figure 2. Profile of ocean botton looking east

Figure 3. Photograph of Antenna Tower.

TABLE I

Parameters of 3-mm Radar

Transmitter:	
Tube type:	Amperex DX 287
Frequency:	95 GHz (nominal)
Peak power output:	4 kW (nominal)
Pulse length:	100 ns (nominal)
PRF:	1500 Hz
Receiver:	
Local oscillator:	Oki 90V10
Mixer:	Balanced, Adtec M995B
Noise figure:	(See Chapter V)
Intermediate frequency:	120 MHz (nominal)
I-F bandwidth:	40 MHz (nominal)
Output pulse length:	80 ns (-3 dB level)
Envelope transfer characteristic:	Logarithmic
Duplexer:	
Components:	4-port circulator plus ferrite switch crystal protector
Isolation:	20 dB
Switch protection:	40 dB
Loss:	5.5 dB total (switch 1.5 dB; circulator 4.0 dB 2-way)
Antenna:	
Design:	Cassegrain
Diameter:	24 inches
Polarization:	HH or VV
Beamwidth:	0.38 x 0.38 deg.
Gain:	53 dB (nominal)
Height:	75 feet
Mount:	Azimuth-over-elevation positioner

The radar cell area is required in order to relate the clutter cross section to the quantity σ°. For purposes of data reduction, the cell area was defined to be

$$A_c = \frac{c\tau\theta_a R}{2\sqrt{2}} , \tag{3}$$

following Barton [6], in which θ_a and τ are the 3-dB one-way azimuth beamwidth and pulse length, respectively, and R is the range. Using τ = 80 ns and θ_a = 0.38 degree, the cell area at 1 μs range is found to be 8.4 m^2 (corresponding to +9.3 dBsm).

2. X-Band Radar. The experimental X-band radar was constructed by personnel of the Georgia Institute of Technology on Contracts NObsr-91024 and N00024-68-C-1125. Parameters pertinent to this experiment along with others of interest are listed in Table II. Under normal conditions, the transmitter parameters would have been:

Tube type	Raytheon QK-369
Peak power output	250 kW
Pulse length	0.12 μs
PRF	4 kHz

However component failures precluded use of the final amplifier. No disadvantage was incurred though because of the inherent short range of the 3-mm radar, and adequate power was available using the 2J42 driver magnetron.

The X-band radar has been calibrated by observing standard-sphere targets elevated well above the sea surface. Calibrations performed over widely spaced intervals and with two different targets agree within 0.5 dB, and the constants are believed known to within 1.5 dB of correct value. The calibration constant for the radar of Table II is expressed in the form such that the power received from a 1-m^2 target at a range of 1 μs is -7.3 dBm. Individual measurements are calibrated with a secondary standard to which the above sphere returns were referenced. This standard is an X-band signal generator with internal precision attenuator (Dymec 5003). Periodic calibrations of its output power delivered to the receiver are made using separate power meter standards. Closure errors over long time periods have not exceeded 1 dB.

TABLE II

Parameters of X-band Radar

Transmitter:	
Tube type:	2J42
Frequency:	9375 MHz
Peak power output:	5 kW
Pulse length	0.4 μs
PRF	1500 Hz
Receiver:	
Mixer:	Balanced using 1N23E point-contact diodes
Intermediate frequency:	60 MHz (nominal)
IF bandwidth:	10 MHz (nominal)
Envelope transfer characteristic:	Logarithmic
Duplexer:	
Components:	4-port circulator plus gas tube crystal protector
Antenna:	
Design:	Cut paraboloid with solid reflector
Dimensions:	10 x 3.5 feet
Polarization:	VV or HH
Beamwidths:	0.8 x 2.2 degrees (Az x El.)
Gain:	41.5 dB (nominal)
Height:	75 feet
Mount:	Azimuth rotation only

The X-band radar configuration used in these experiments had pulse length 0.4 μs and azimuth beamwidth 0.8 degree (3-dB, one-way), which with Equation 3 calculates a clutter cell area of 88.9 m^2 (corresponding to +19.5 dBsm) at a range of 1 μs.

B. Data Recording Instrumentation

A block diagram of the video processing equipment is shown in Figure 4. Video signals from the appropriate radar were sampled with an aperture of ≈20 ns at a time chosen by the range delay generator. The voltage representing the received signal at that time is stretched, adjusted in gain and offset, and sorted with a Fabritek-Industries Model 1072 Instrument Computer. The distribution-analyzed data could be checked for validity with the x-y oscilloscope and were plotted for retention and later analysis. The Fabritek computer contains hardwired scaling and integration functions so that the data plotted were in the form of cumulative distributions.

Only a single channel of sampling, A-to-D conversion and memory bank (256 words) was used, so that calibration (with corner reflector or signal generator) and acquisition of target signal data from the two radars were accomplished serially. Target data runs were taken with antennas fixed and pointed at the target and returns were sampled and sorted at the pulse repetition frequency over an interval of 160 sec. Calibration runs were limited to 20 sec in length because of the lower inherent fluctuation of the signal. Four quadrants of memory of 256 words each were available for rapid sequencing of data runs before readout was required.

Additional data were recorded manually on a log form, a copy of which is in Appendix B. Wind speed instrumentation consisted of anemometer and Bernoulli wind gauges mounted 55 and 75 feet above the water, respectively, and such as to be reasonably exposed for winds from North around through East to South. Wave height was estimated visually; unfortunately the recording wave gauge normally available was damaged immediately prior to these experiments, and repair was not accomplished during this period.

C. Data Acquisition and Reduction Procedure

The procedures used differed for the two radars because of the calibration methods, so they are described separately.

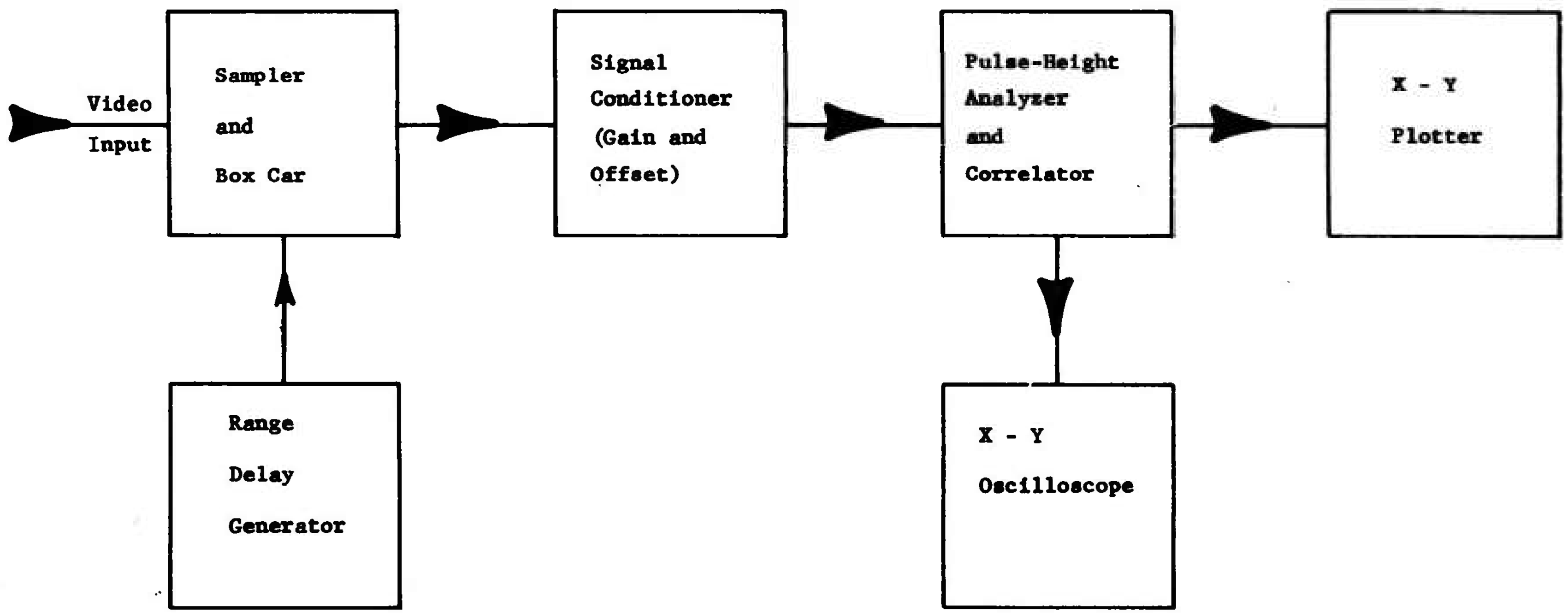

Figure 4. Video Processing Equipment.

1. 3-mm Radar. In setting up to record data, the antenna would be boresighted on the target of interest, and the range gate positioned such that the sampling gate pulse was coincident with the peak of the return pulse. Distribution analyzed data were accumulated for the appropriate length of time (160 sec for target signals and 20 sec for calibration runs were typical). Supporting data were recorded manually and both the log entry and cumulative distribution plot were assigned a serial run number in a new sequence for each date. A sequence of runs was made boresighted on the corner reflector with different receiver-input attenuator settings to establish a calibration curve for the video voltage. This calibration sequence was repeated at least once each day and other check runs were interspersed more frequently within the target data runs.

In Figure 5 is reproduced a calibration sequence of distributions. The abscissa is labeled with memory channel number (0 to 255) corresponding to video voltage, and, hence, also input power expressed in dB. The ordinate corresponds to cumulative probability that the signal is less than the abscissa value. The curves are seen to be approximately normal with a standard deviation on the order of 2 dB. Thus, the median is a good estimate ot the level corresponding to the average input power of the receiver. (This is especially true here because some of the spread is produced by hum and noise introduced after logarithmic envelope detection.) In Figure 5 the handwrittern figures are run numbers and the corresponding receiver input-attenuation figures are typed near the curves.

The distance from the left axis to the median of each calibration curve was read in inches and used to plot a calibration curve. By two successive applications of a Gaussian interpolation program (HP Part No. 09100-70010) on a calculator (HP 9100A) the corresponding distances to points on target return curves were converted to equivalent input-attenuator settings in dB with the accuracy of cubic interpolation between the calibration points.

The statistic of greatest interest to the study of deterministic dependences of $\sigma°$ is the average of the received target power. Because the received power fluctuates widely, the median is a poor estimator of the average power. The clutter and target signal distributions fluctuate over more dynamic range than does the Rayleigh distribution, so the known properties of the latter are not suitable for location of the average. It

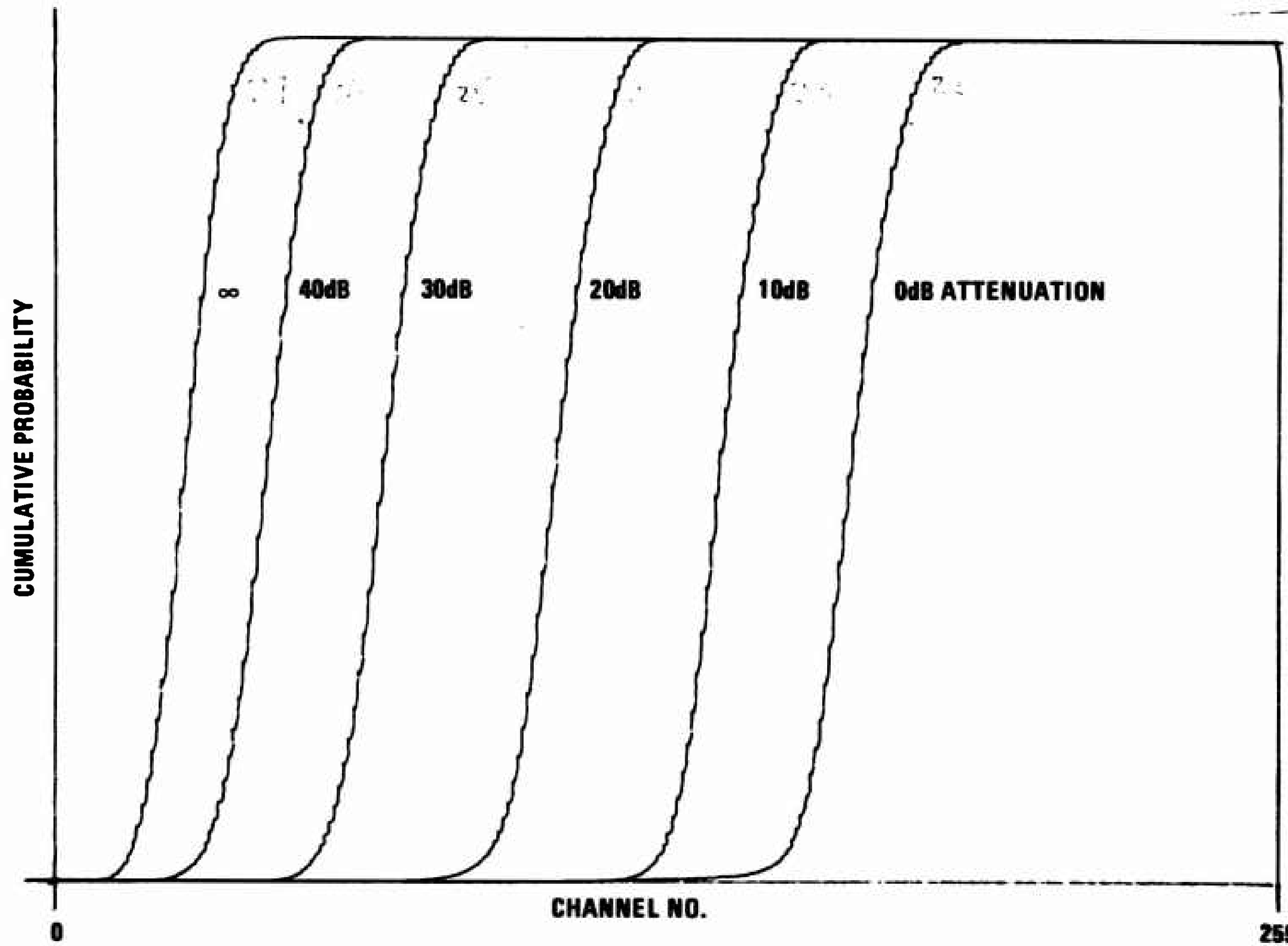

Figure 5. Calibration Data from 3-mm Radar.

has been found that for some distributions of the type encountered with sea-return signals, the average power lies 3.5 $\pm$ 0.5 dB below the power level corresponding to the 0.9 cumulative probability. Some supporting argument for this rule is offered in Appendix A. This rule has been applied uniformly in the reduction of data from this experiment. The attenuator settings corresponding to the 0.9 probability abscissa distances of the target signals were computed using the interpolation of the corner-reflector-and-attenuator calibration data. To these dB values 3.5 dB was added (corresponding to lower effective input power), and the resulting attenuation value designated as that required to reduce the corner-reflector signal to be equal to the average target-signal power. Call that value L'_t.* Then the target cross section in dBm was calculated from

$$\sigma'_t = \sigma'_s - L'_t - 40 \log R_s(\mu s) + 40 \log R_t(\mu s). \tag{4}$$

Recall that σ'_s = +10.4 dBsm and R_s = 4.55 μs (corresponding to 2240 feet), so that

$$\sigma'_t = -15.9 \text{ dBsm} - L'_t + 40 \log R_t(\mu s), \tag{5}$$

where L'_t is an attenuation in dB and is greater than zero. The value of $\sigma°$ (in dB) is related to σ'_t by

$$\sigma° = \sigma'_t - A'_c , \tag{6}$$

or, recalling that A'_c = + 9.3 dBsm + 10 log $R_c(\mu s)$,

$$\sigma° = -25.2 \text{ dB} - L'_c + 30 \log R_c(\mu s). \tag{7}$$

Subscripts in the above denote standard corner by "s", clutter by "c", target by "t", and the target may be a clutter patch or an object on the sea.

2. X-band Radar. Calibration procedure differed for this radar because a signal generator was used to inject signals of known power into the

*The prime notation here distinguishes a quantity expressed in dB from one which is a pure ratio. $\sigma°$ is an exception and is always in dB where written as a number in this report.

receiver input, and no antenna aiming on a standard target was required. Setting the signal-generator attenuator to levels 10 dB apart results in a cumulative distribution of the video voltage like that in Figure 6, run 21. The median of each step served as before to represent the power level, and interpolation was used to compute the power level of the 0.9-cumulative abscissas of the target data curves. The 3.5-dB rule was applied by subtracting 3.5 dB from the 0.9 probability power level to find the estimated average power in dBm. Call this average power P_t'. Then the target cross section in dBsm was computed from

$$\sigma_t = P_t' \text{ (dBm)} + 7.3 + 40 \log R_t(\mu s) + F'(\theta), \tag{8}$$

where $F'(\theta)$ is a correction for the antenna elevation beam shape.* Recall that A_c = +19.5 dBsm + 10 log $R_t(\mu s)$, so that

$$\sigma^\circ = P_t'(\text{dBm}) - 12.2 \text{ dBm} + 30 \log R_c(\mu s) + F'(\theta) . \tag{9}$$

The antenna beam-shape correction is required because data were taken at short ranges such that some reduction in illumination of the surface resulted because of the horizontal boresight plane and finite elevation-plane beamwidth. The 2-way correction function in dB is given approximately by

$$F'(\theta) \simeq 6\left(\frac{2\theta}{\theta_e}\right)^2, \tag{10}$$

where θ is the depression angle below boresight of the target vector, and θ_e is the one-way 3-dB beamwidth in the elevation plane. For horizontal aiming, $\theta \simeq h_a/R_t$; h_a = 75 feet, $R_t(\text{ft}) = \frac{6000}{492} R_t(\mu s)$ and θ_e = 2.2 deg. = 3.84×10^{-2} radians. Thus,

$$F'(\theta) = F'(R_t) = \frac{381}{R_t^2(\mu s)} \tag{11}$$

*The radar calibration constant is expressed by, "the power received from a one-square-meter target at a range of one-microsecond range is -7.3 dBm."

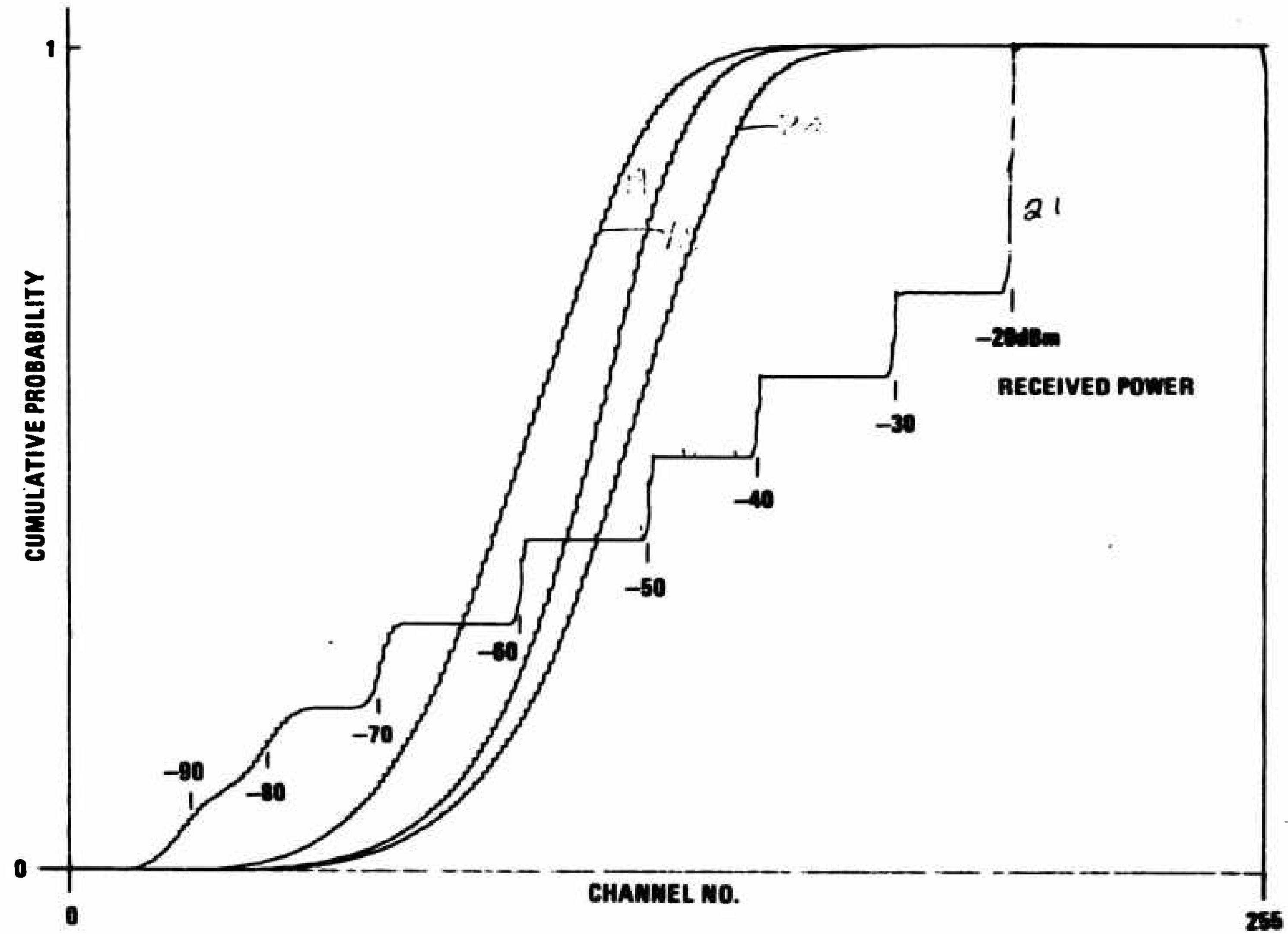

Figure 6. Calibration and Clutter Data from x-band Radar.

III. RADAR SEA RETURN

This chapter presents the results of measurements on sea return; most of the data presented are for 3-mm wavelength. The chapter is organized into two sections. The first concerns the deterministic behavior of σ° with changes in selected variables (depression angle or range, wind speed, polarization, wavelength and angle between boresight and wind vector), and the second deals with the statistics of sea return (probability distributions and autocorrelation functions).

A. σ° And Its Dependences

1. Range Dependence. The incidence-angle dependence of σ° is implicitly contained in the range dependence, and, for low grazing angles and at ranges short compared to the horizon distance, the relationship is a simple one, with the grazing angle of incidence being inversely proportional to range. However, because the data were recorded as a function of range, they are presented as a function of range, and it should be understood that interpretation in terms of the angle variable may include pure range-dependent effects such as nonhomogeneity of the environment.

Figures 7 and 8 summarize the data for horizontal and vertical polarizations, respectively. The data were extracted from the totality of those cases in which runs stepped in range were blocked closely in time so that the effects of changing conditions were minimized. All wind speeds and look directions encountered are included in these plots of σ° in dB against range on a logarithmic scale.

Interpretation of the data requires reference to the table of partially reduced data in Appendix B. In Figures 7 and 8 the first number of each curve is the day of the month, and the last two are the run numbers beginning and ending the sequence. The final letters, U and C, indicate upwind and crosswind look directions, respectively. In Table III below, the wind speeds and wind and boresight directions have been extracted from Appendix B. By comparing Figures 7 and 8 with the conditions in Table III, there is seen to be some correlation between the type of range law observed and the sea state and look direction. The trend is that, looking upwind into stronger winds, σ° falls off somewhat with range, whereas looking away from upwind

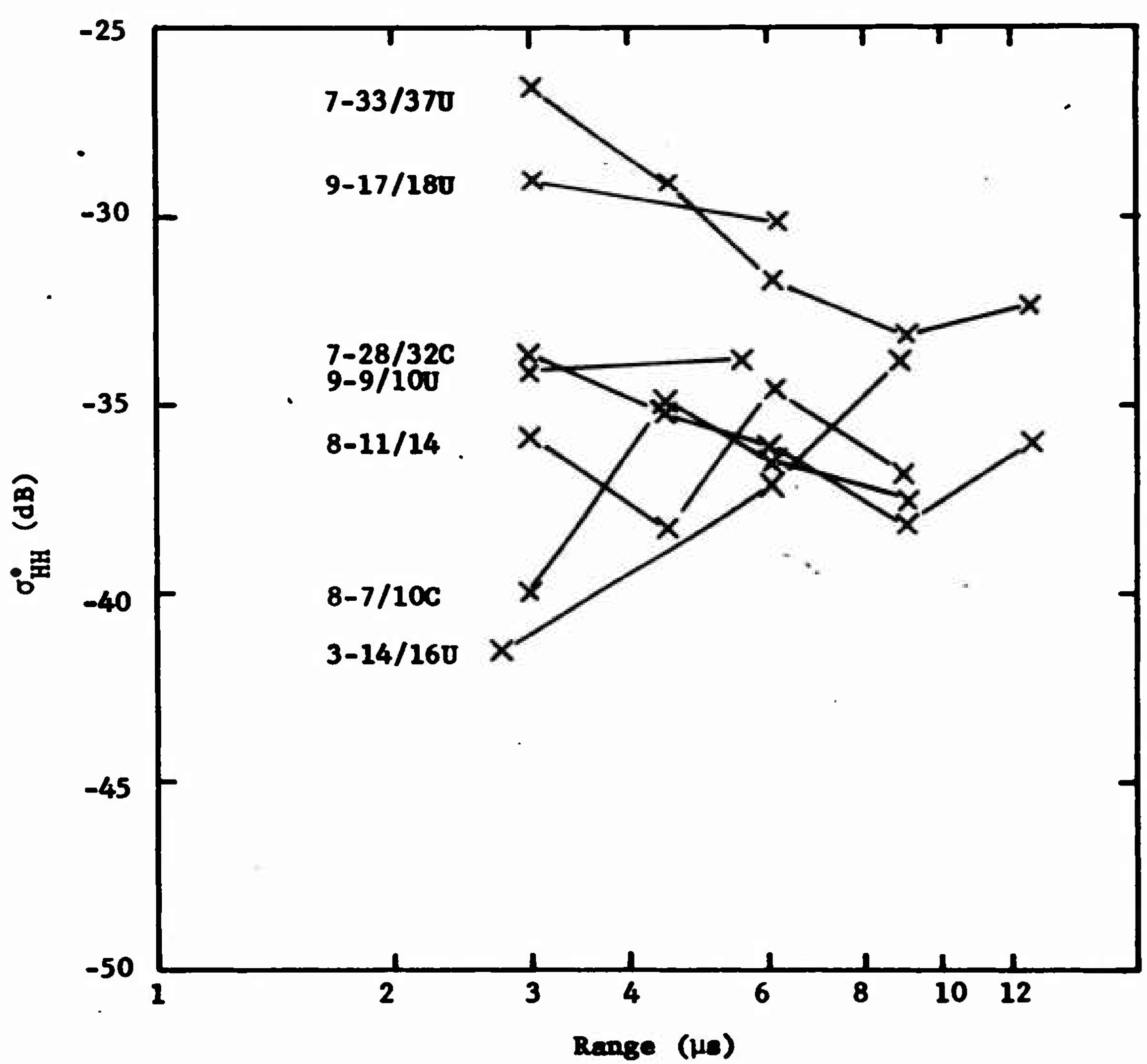

Figure 7. Range dependence of σ^o_{HH}; λ=3mm, horizontal polarization

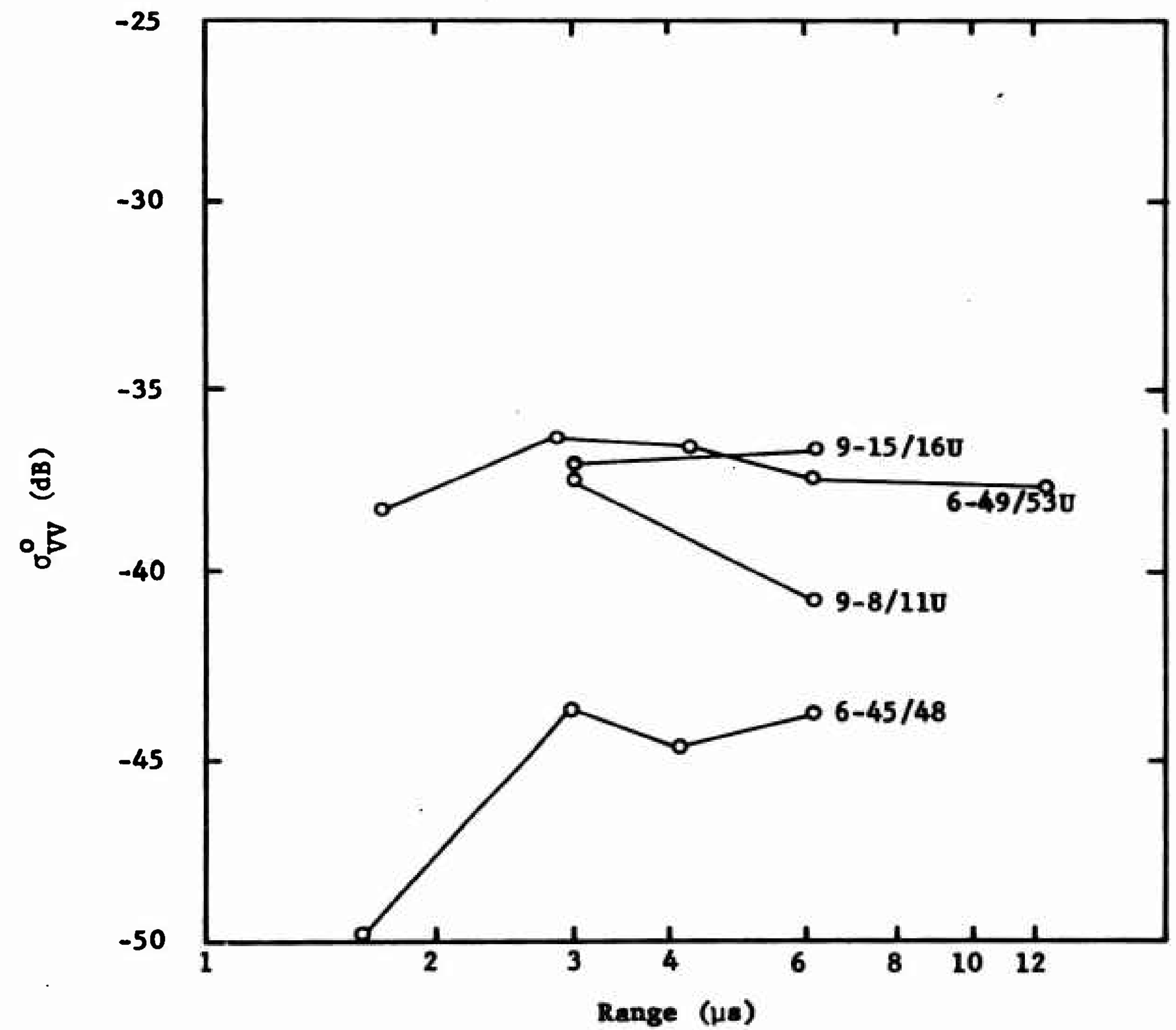

Figure 8. Range dependence of σ°_{VV} ; λ=3mm, vertical polarization

or in lower sea states the trend is for σ° to remain approximately constant or to increase with range. This increase may be the result of deepening water farther off shore allowing somewhat longer period surface waves and perhaps higher crests there. It should be noted that 3-μs range corresponds to an incidence angle of 2.9 degrees, and 12.4 μs range corresponds to an angle of 0.7 degrees; these two angles bound most of the data taken.

TABLE III

Conditions for Data of Figures 7 and 8

Date-Runs	Wind	Look
3-14/16	6 kts - 150 deg	150 deg
6-45/48	7 - 135	090
6-49/53	7 - 135	135
7-28/32	12.5 - 135	090
7/33/37	12 - 135	135
8-7/10	12 - 180	095
8-11/14	12 - 180	140
9-8/11	9.5 - 150	140
9-9/10	9.5 - 150	140
9-15/16	12.5 - 150	140
9-17/18	12.5 - 150	140

2. Wind-Speed Dependence. Data at 3-mm on σ° extracted for ranges of 6 μs and 3 μs are plotted in Figures 9 and 10, respectively, against wind speed on a logarithmic scale. The data points are marked with a code, the first number of which is the date, the second is the run, and the terminal letter designates whether the look direction was upwind (U), crosswind (C) or somewhere in between (no letter). The two polarizations are distinguished by the symbols plotted, X for horizontal and O for vertical.

A few trends are clear in these figures. σ° tends to increase with wind speed. Selecting the points for upwind look direction and horizontal polarization in Figure 9, one finds that a line with slope 1.5 is a fair fit to the 6-μs data. The same slope is representative of the upwind vertical-polarization points also, but the line would be offset about 5 dB lower

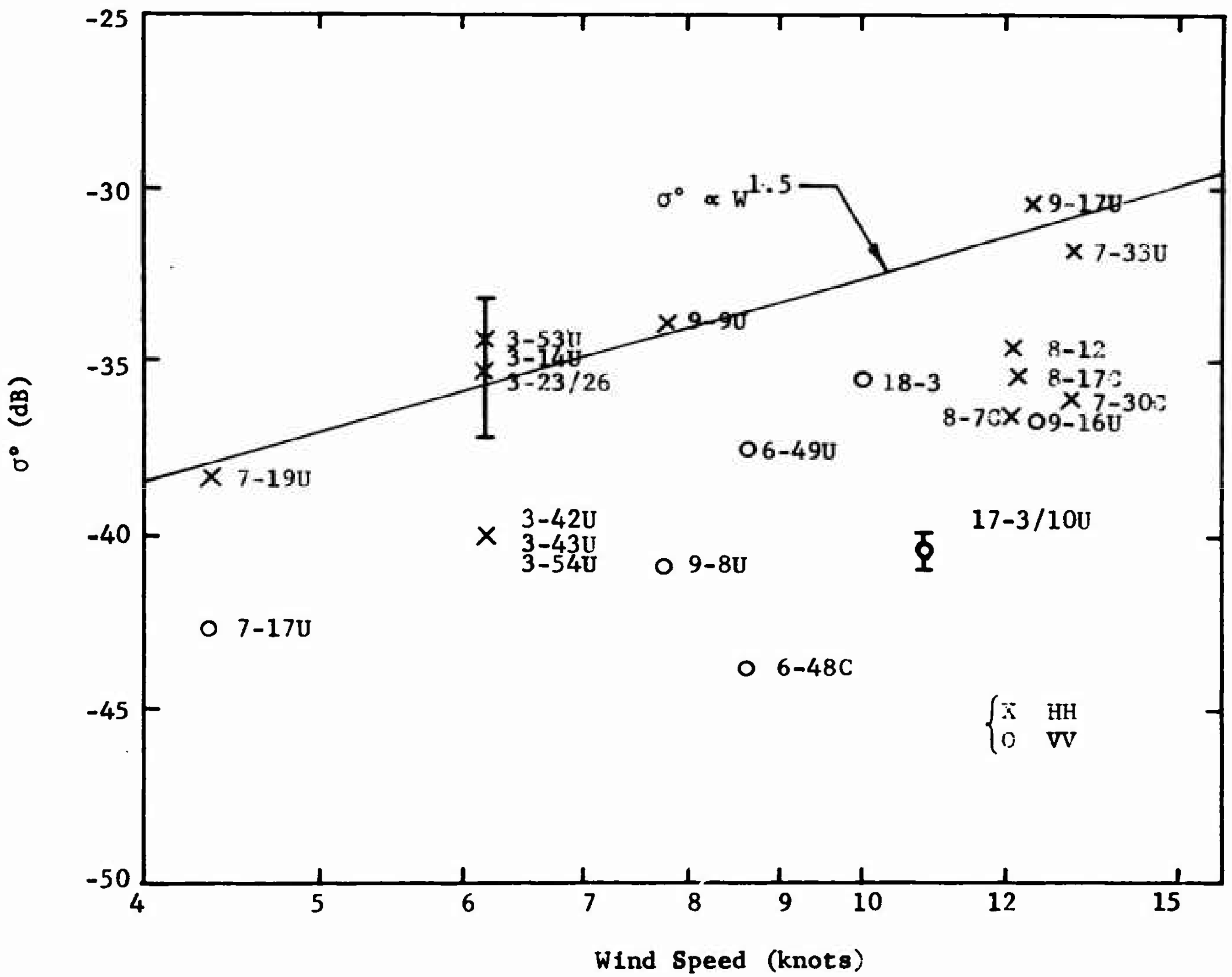

Figure 9. Wind-speed dependence of $\sigma°$; λ = 3mm, range = 6.2 μs

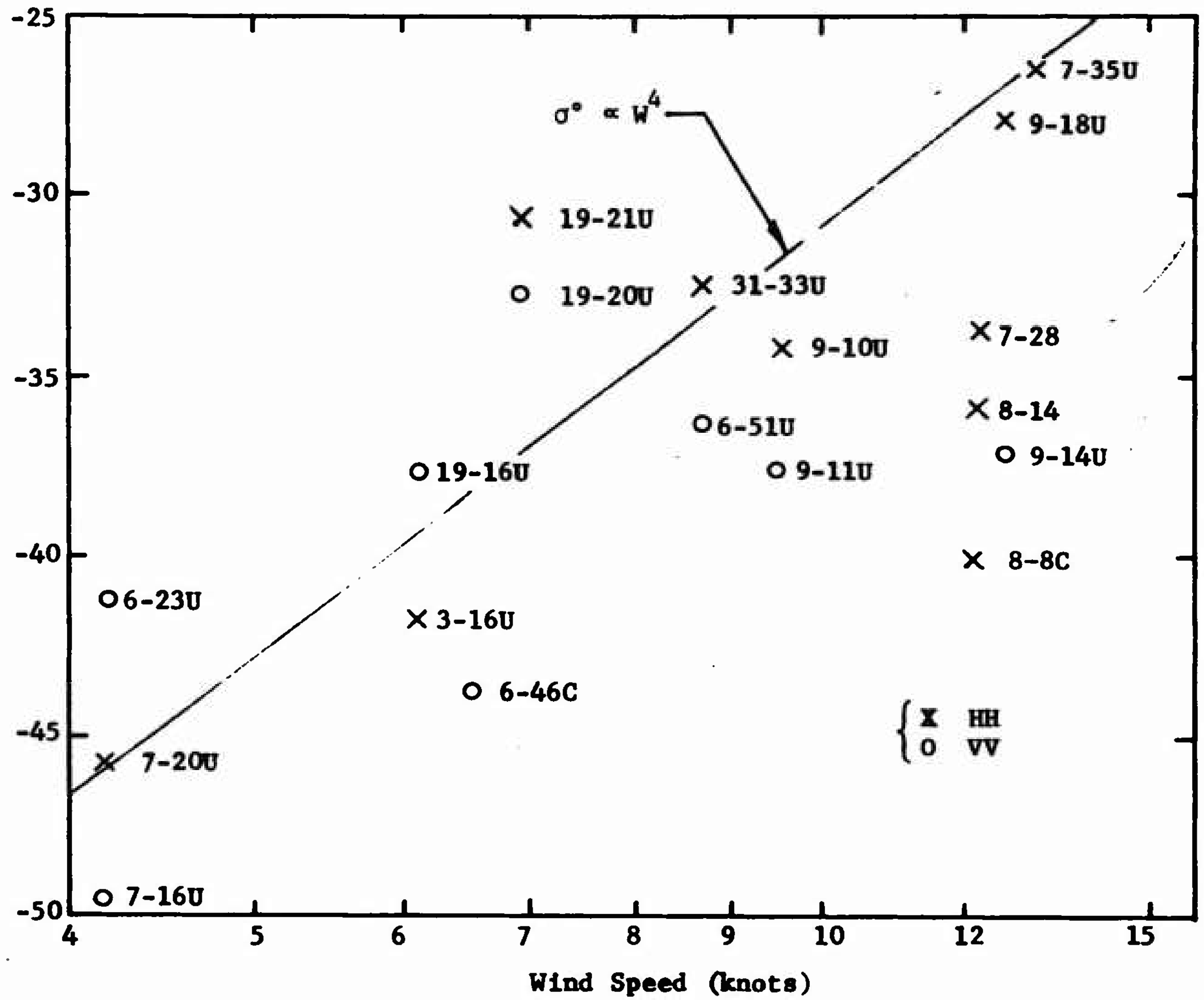

Figure 10. Wind-speed dependence of σ°; λ = 3mm, range = 3.0 - 3.2 μs

than for horizontal. There are not enough crosswind data spread over a wide enough span of wind speed to establish slope, but it is clear that the crosswind points tend to lie lower on the $\sigma°$ scale than the upwind points.

At a range of 3 μs, corresponding to an incidence angle of 2.9 degrees, the spread of data is somewhat greater, but the same trend for $\sigma°$ to increase with wind speed is clear, and the slope seems to be greater, about 4. The tendencies for vertical and crosswind look-direction points to lie below horizontal and upwind points is also followed as at 6-μs range.

3. Polarization. Data are plotted in Figure 11 for those runs taken under the same conditions and at the same range and look direction but immediately before and after a change of polarization. All ranges, look directions and wind speeds encountered are represented in these data. Other data from Appendix B could have been plotted but would not satisfy the criterion of near simultaneity. The median ratio, $\sigma^{\circ}_{HH}/\sigma^{\circ}_{VV}$, for the points plotted is 4.5 dB (σ°_{VV} smaller than σ°_{HH}) the average is 4.8 dB, and the standard deviation is 2.3 dB. The minimum ratio observed was 0 dB and the maximum was 8.5 dB.

4. Wavelength Dependence. Data were chosen from Appendix B for situations in which X-band and 3-mm runs were made under the same conditions, polarization, and look direction and at a range of 6 μs (corresponding to an incidence angle of 1.4 degrees). They are plotted in Figure 12, with the value of $\sigma°$ at 3.2 cm along the abscissa and the value of $\sigma°$ at 3 mm along the ordinate. Both polarizations are represented in the data.

The transition angle below which forward-scattered interference effects seriously modify sea return is given approximately by [14]

$$\psi_c = \frac{\lambda}{6.3\ h_{av}}, \qquad (12)$$

where h_{av} is the average wave height. For ψ_c at 3.2 cm to lie at or below 1.4 degrees, h_{av} must be equal to or greater than 0.7 feet. Thus, for those conditions when $h_{av} \geq 0.7$ feet, both radars would have observed clutter in the "plateau" region of the angle domain. Because no wave-height instrumentation was available and only visual estimates could be made, there is considerable quantitative uncertainty about the conditions that existed. However, it is believed that the data points in the left half of Figure 12

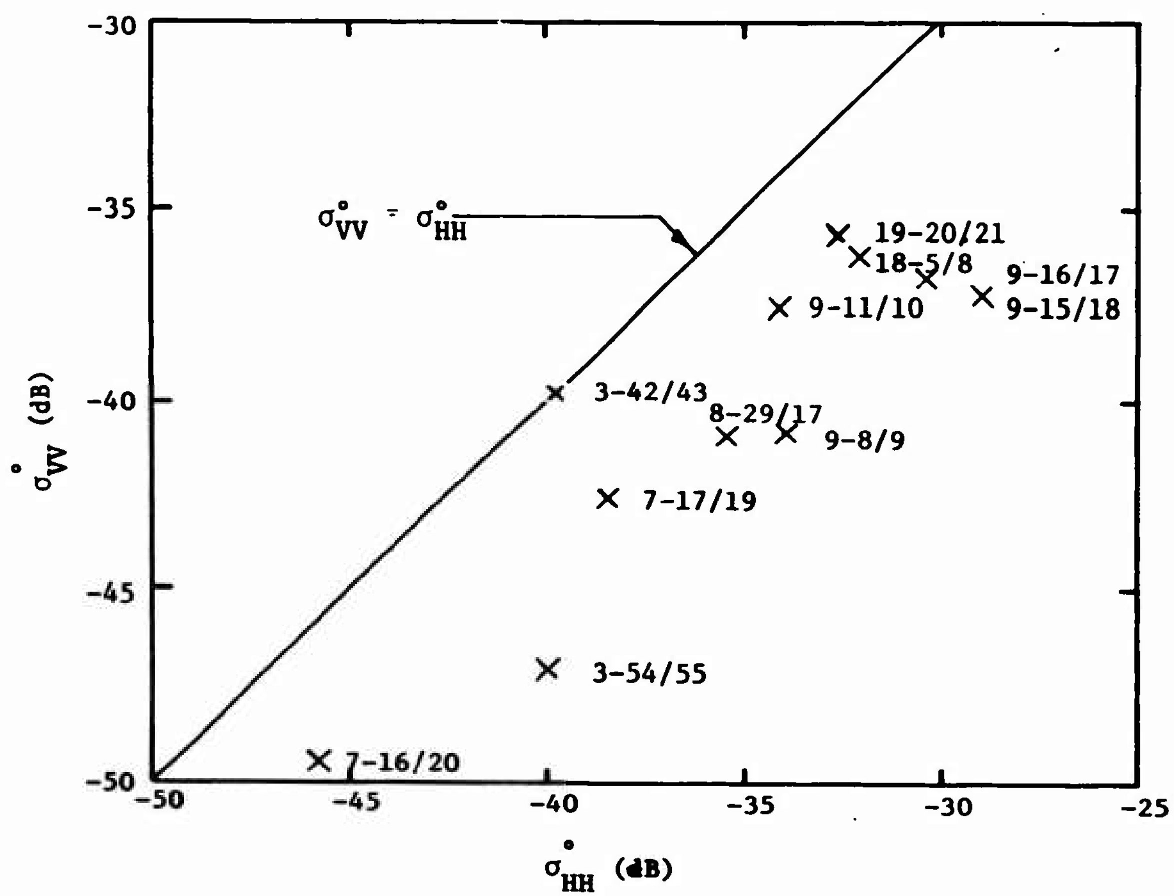

Figure 11. Scatter diagram of σ° for vertical and horizontal polarization; λ = 3 mm

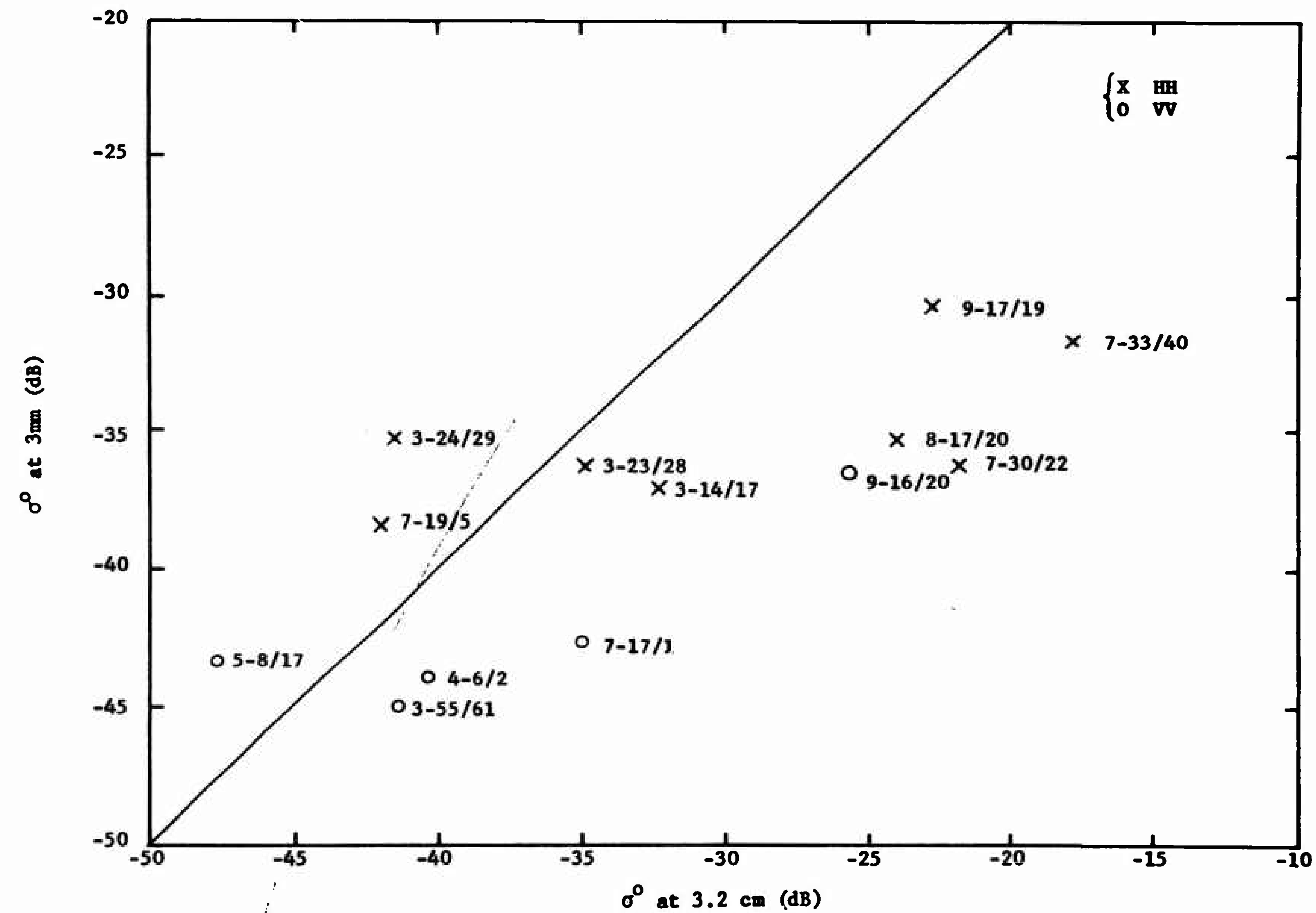

Figure 12. Scatter Diagram of σ^{o} at 3-mm and 3.2 cm; Range = 6 μs.

are for wave heights of 0.7 feet or slightly greater, and those on the right half are for wave heights substantially greater than this transition value. It cannot be said with any degree of certainty that all the data apply to the plateau region.

From the figure it appears that σ° at 3 mm increases as σ° at 3.2 cm increases, that points for vertical polarization lie below those for horizontal, and that σ° at 3 mm is on the same order as that at 3.2 cm at low sea states. However, it appears that σ° at 3 mm is substantially less than that at 3.2 cm for the higher wind speeds which occurred on 7, 8, and 9 August.

5. Angle Between Boresight and Upwind Directions. The data from these experiments are confusing with respect to establishing the relationship between σ° and the wind aspect angle at 3 mm. In Figure 13 are plotted two sequences of runs in which aspect angle was varied, with other factors held fixed. The quality of the data taken on 17 August is much better than that on 3 August; taking this into account, one concludes that there is no significant variation of σ° with look direction near upwind. However, contradicting this is a large group of runs not taken close together in time which imply substantial variation of σ° with aspect angle. This trend was pointed out in Figures 7 through 10, and from the data in those figures it appears that the ratio of σ° looking upwind to that looking crosswind is between 5 and 10 dB for both polarizations and for windspeeds above about 9 kts.

B. Statistics of Sea Return

1. Probability Distribution Functions. For certain runs the cumulative distribution functions were recorded from the distribution analyzer in numerical form, which allows much more detailed plotting than the x-y plot records used for most of the data. The cumulative distributions are shown in Figures 14 through 18, in which the probability that the clutter return (expressed as cross section) lies below a threshold level is plotted against that level in dB. The abscissa corresponds to cross section per unit area of the cell and is calibrated so that σ°, the average, lies 3.5 dB below the 0.9 cumulative level. The ordinate scale is arranged so that a log-normal distribution plots as a straight line. Each figure contains two curves for the two polarizations recorded at a given range. There are two sets each at 3- and 6-μs range for the 3-mm radar and one

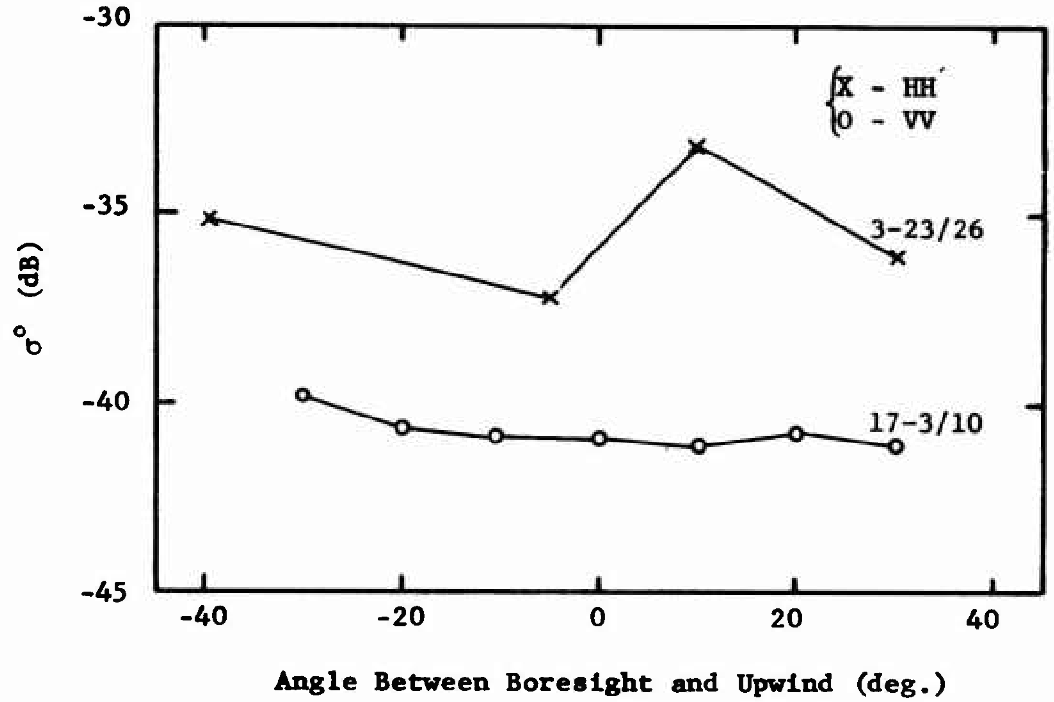

Figure 13. Dependence of σ° on angle between boresight and upwind; λ = 3 mm, range = 6 μs

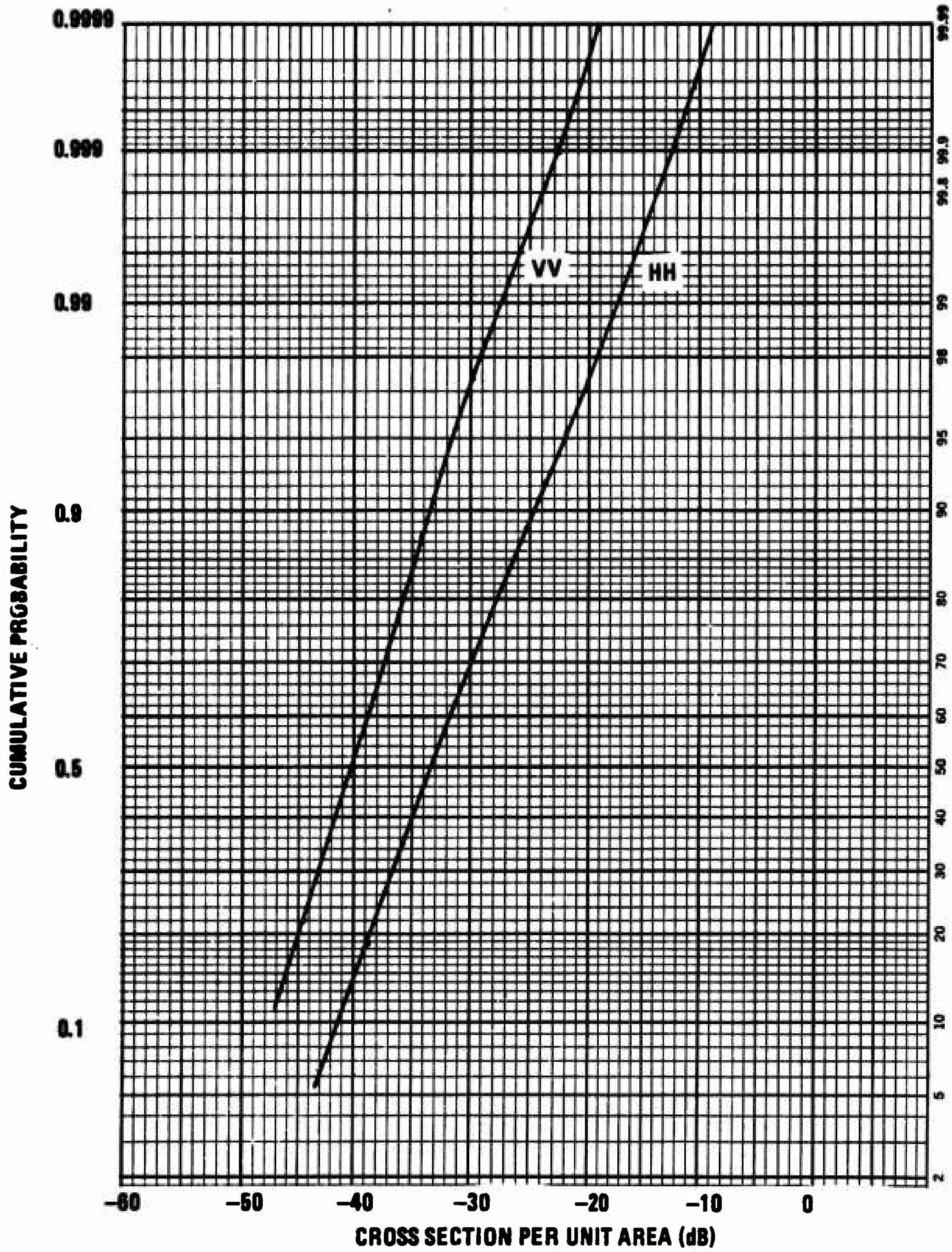

Figure 14. Cumulative Distribution of 3-mm Sea Clutter, Range 3μs, Runs 9-15 and 18.

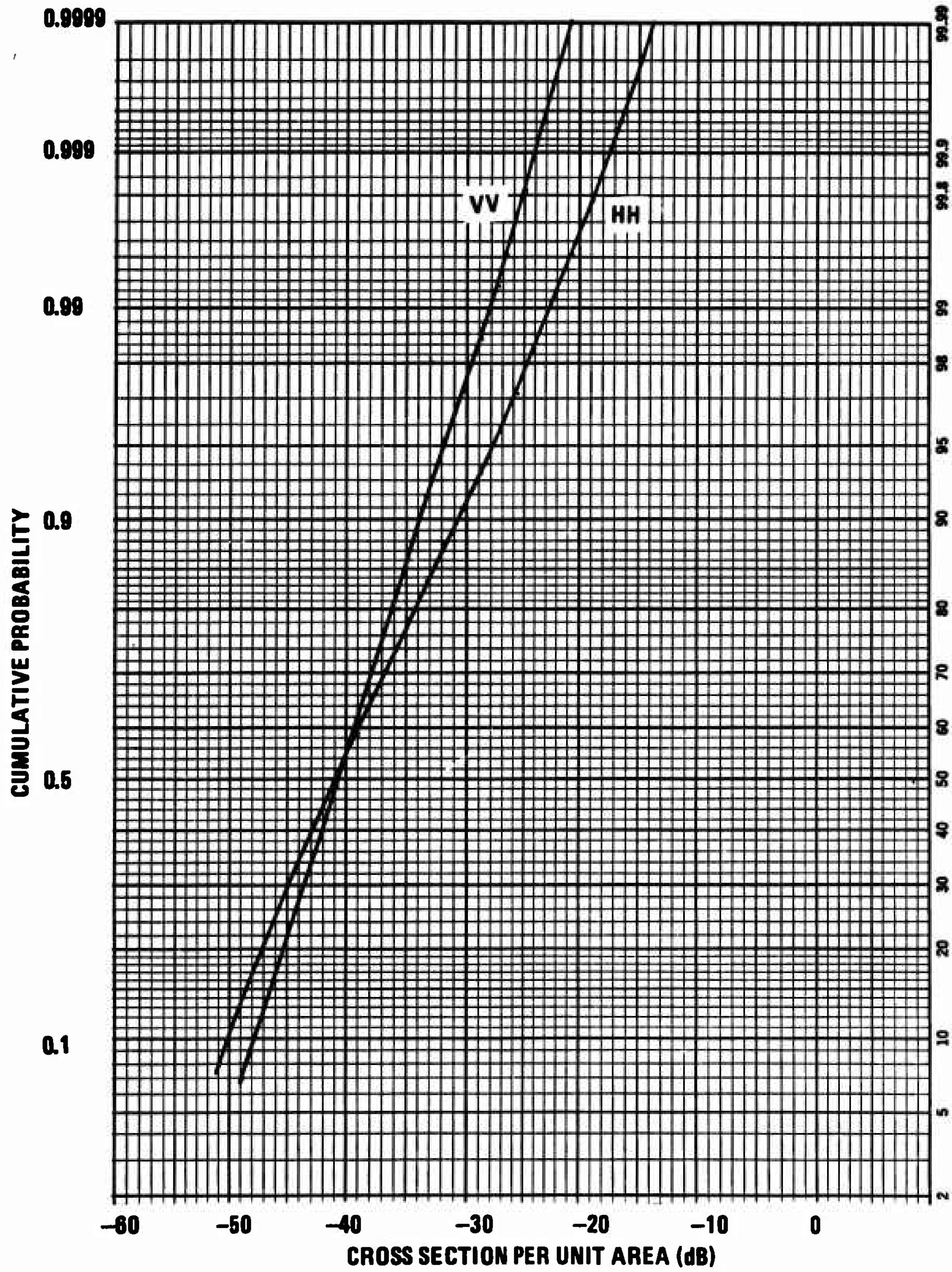

Figure 15. Cumulative Distribution of 3-mm Sea Clutter, Range 3μs, Runs 9-10 and 11.

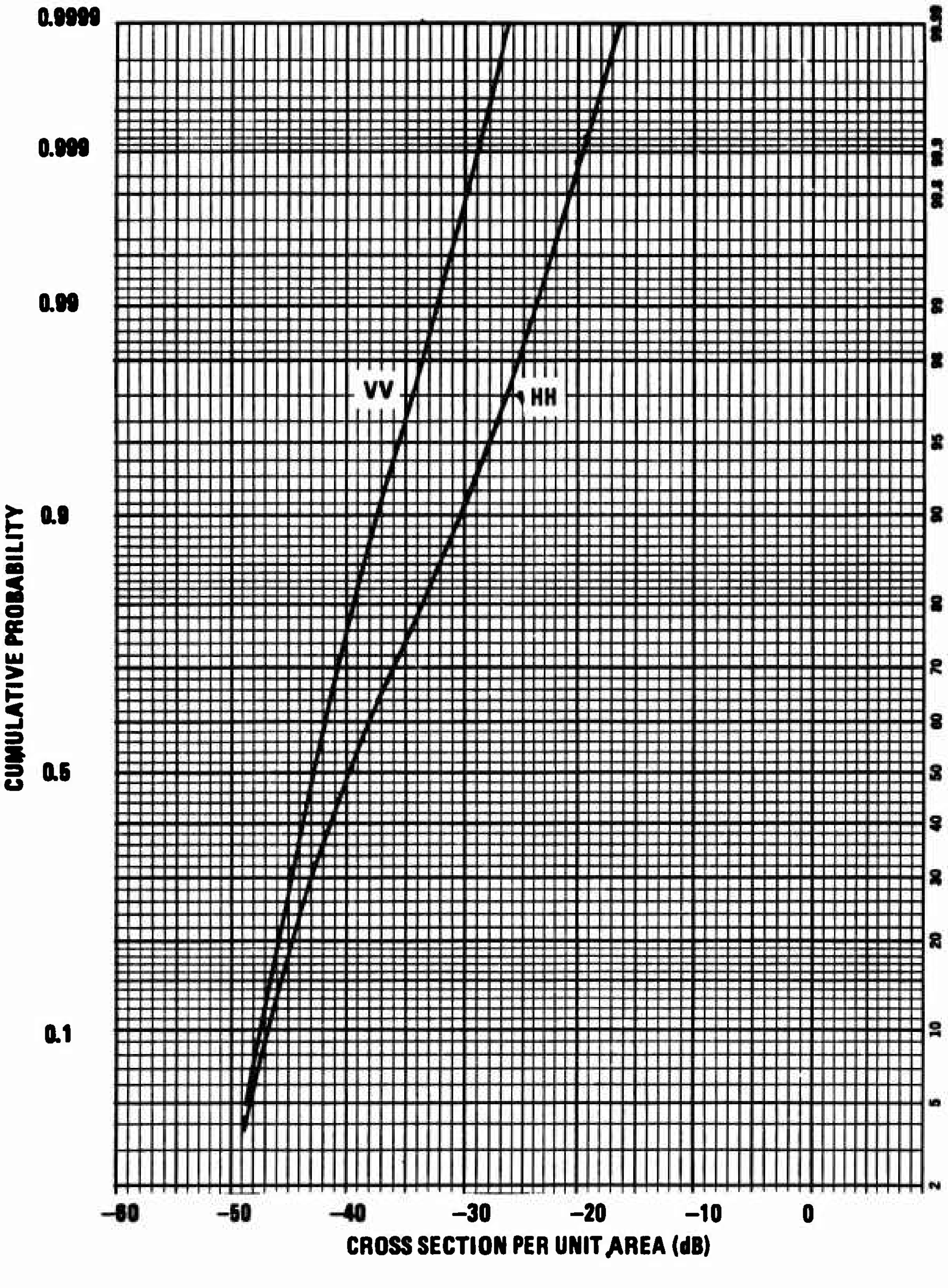

Figure 16. Cumulative Distribution of 3-mm Sea Clutter, Range 6μs, Runs 9-8 and 9.

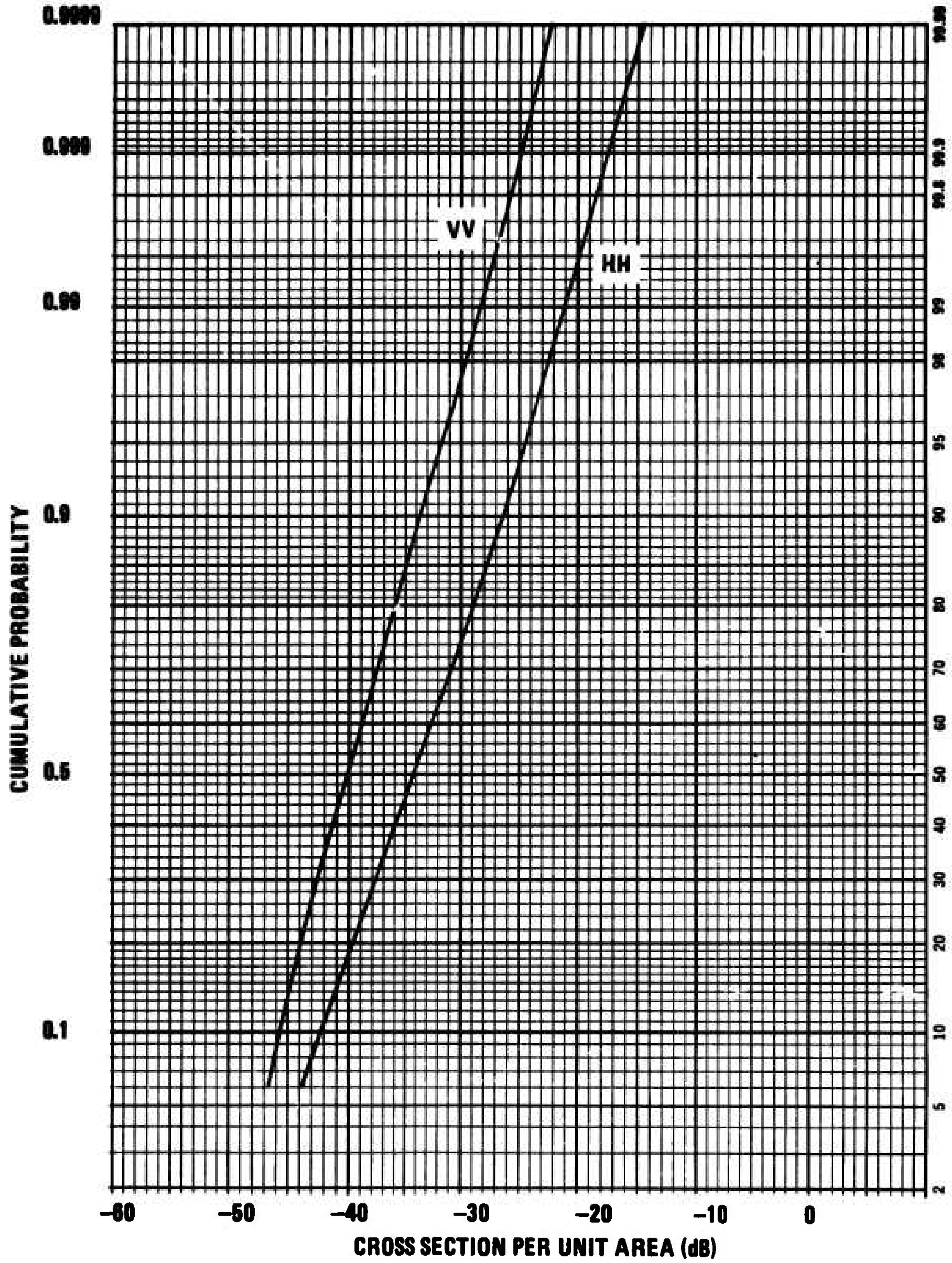

Figure 17. Cumulative Distribution of 3-mm Sea Clutter, Range 6μs, Runs 9-16 and 17.

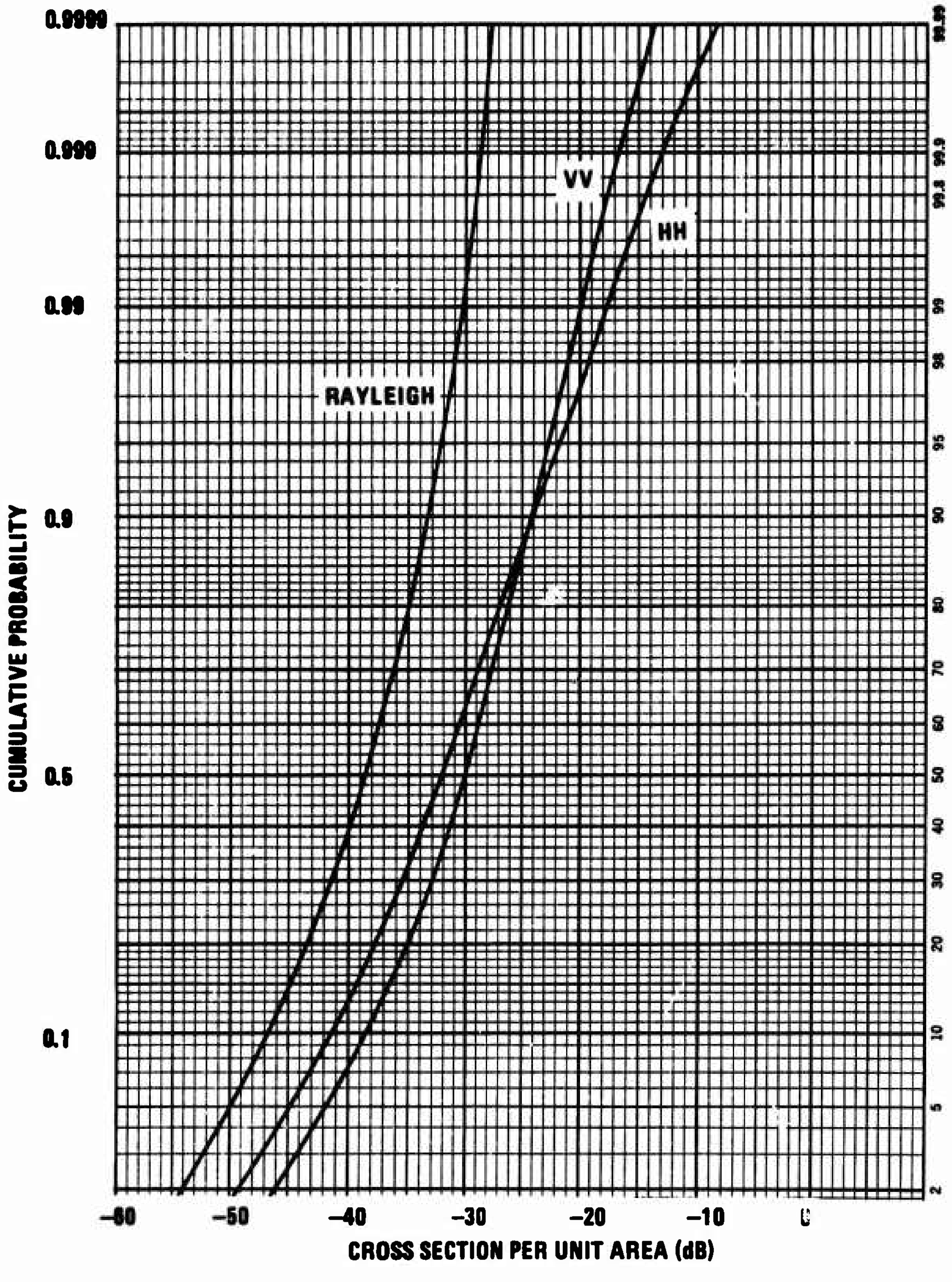

Figure 18. Cumulative Distribution of x-band Sea Return, Range 6μs, Runs 9-12 and 13.

set at 6-μs range for the X-band radar. On Figure 18 along with the X-band curves there is plotted for comparison a theoretical Rayleigh distribution, which is the idealized form of receiver noise at video.

The data for 3-mm clutter show characteristics similar to low-frequency experience. The curves are approximately log-normal above the median, and they have slopes corresponding to standard deviations of about 7.0 $\pm$ 0.6 dB for horizontal and 4.7 $\pm$ 0.6 dB for vertical polarization. These widths are greater than receiver noise, which has a standard deviation of approximately 3.5 dB. The shapes of the 3-mm curves are similar to those for X-band except for the low-power end. The difference here is that the 3-mm video does not show the curved tail on the low side that is characteristic of all noise and clutter distributions and which is produced by the properties of finite bandwidth r-f amplifier filters. The tail is missing in the 3-mm data because the video bandwidth is somewhat narrower than optimum and the negative-going peaks are smoothed by the finite rise time of the video amplifier. The X-band video-amplifier bandwidth had been made intentionally very wide to preserve the statistical effects.

<u>2. Autocorrelation Functions.</u> Using the correlation option of the Fabritek Instrument Computer, estimates of autocorrelation functions were generated, and representative examples are shown in Figures 19 through 22. Figures 19 and 20 are for 3-mm clutter and show the normalized autocorrelation coefficient plotted against time lag. The total lag for the first is 25.6 ms and for the second, 2.56 sec.

Three features of the computation process should be noted before the curves are interpreted. First, the signals are impulse-sampled, boxcar-stretched replicas of target return. The sampling rate was the prf, 1500 Hz, which is low enough so that some of the fluctuation information lies above this frequency, especially at 3-mm wavelength. Second, in order for the random error in the estimate to be tolerable, a low-pass filter with a time constant equal to or greater than the minimum lag interval must be inserted in front of the correlation computer. Thus, the maximum bandwidth visible in the data is in some instances less than the sampling rate. Third, because the video transfer function is logarithmic, a dc offset is inevitable in the video signal. Although effort was made to remove that dc component so that the base line might represent the value

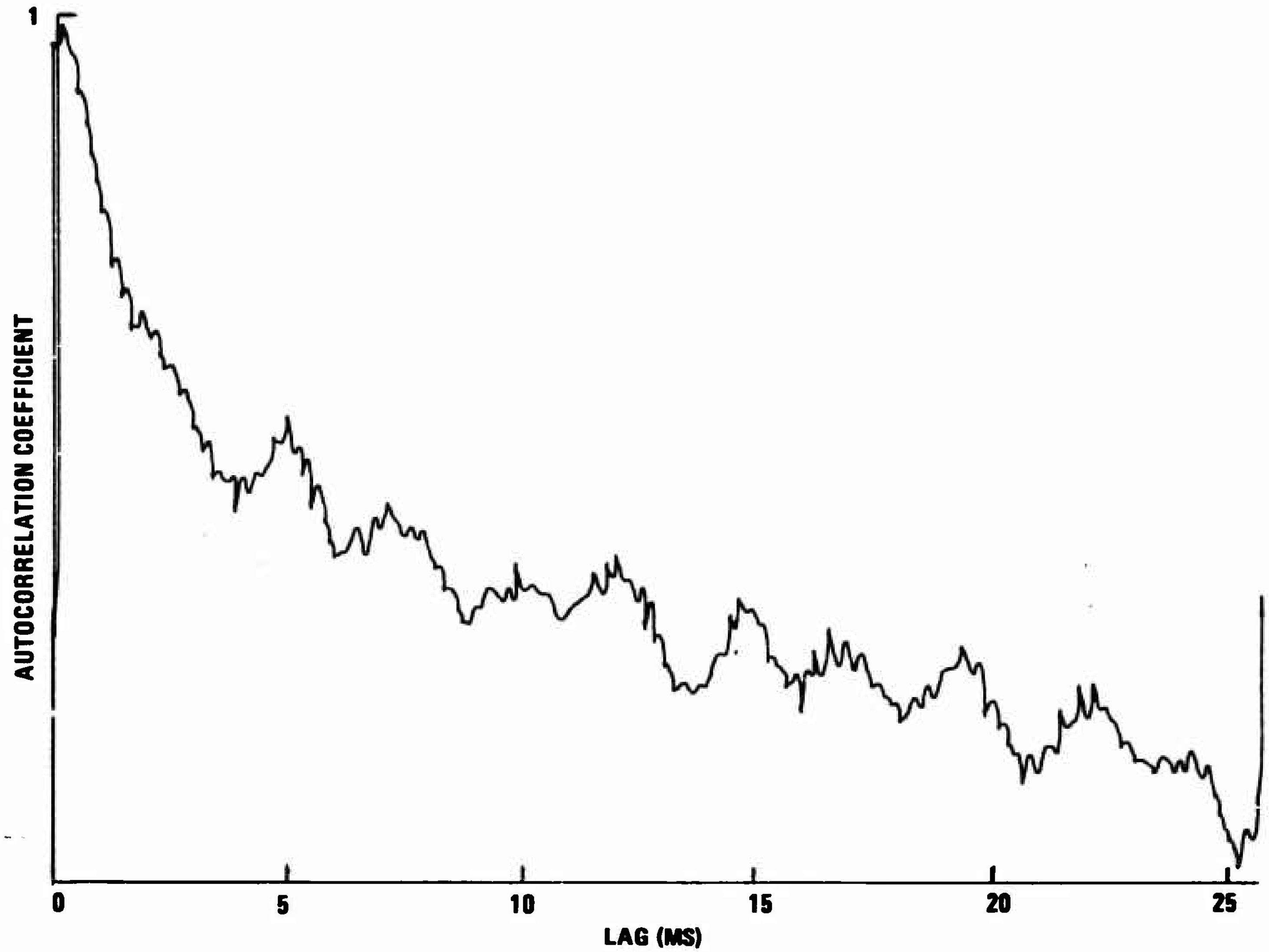

Figure 19. Autocorrelation Coefficient vs. Lag; 3-mm Wavelength; 3μs Range Horizontal Polarization, Runs 9-22.

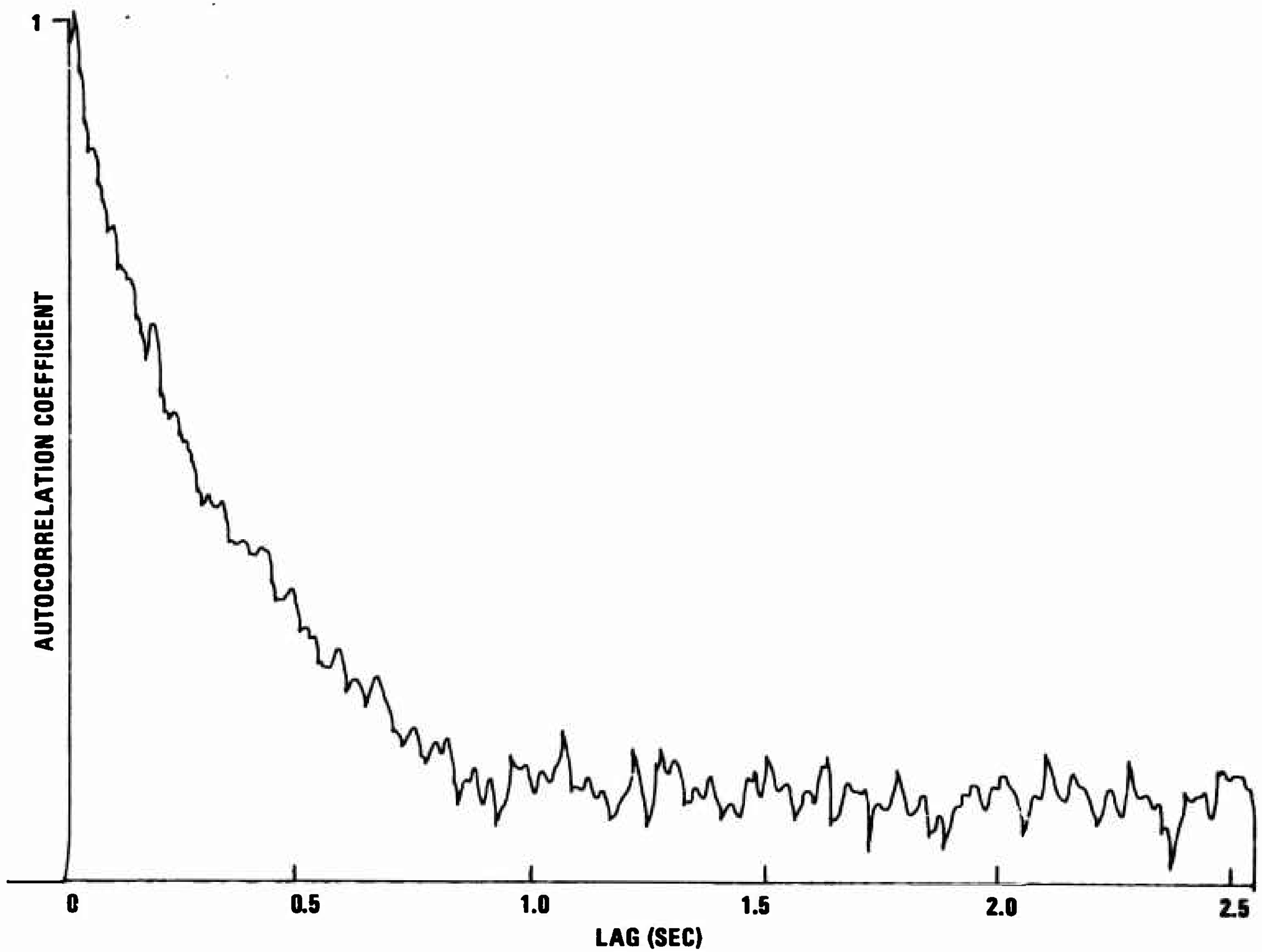

Figure 20. Autocorrelation Coefficient vs. Lag; λ=3-mm, 3μs Range Horizontal Polarization, Runs 19-26.

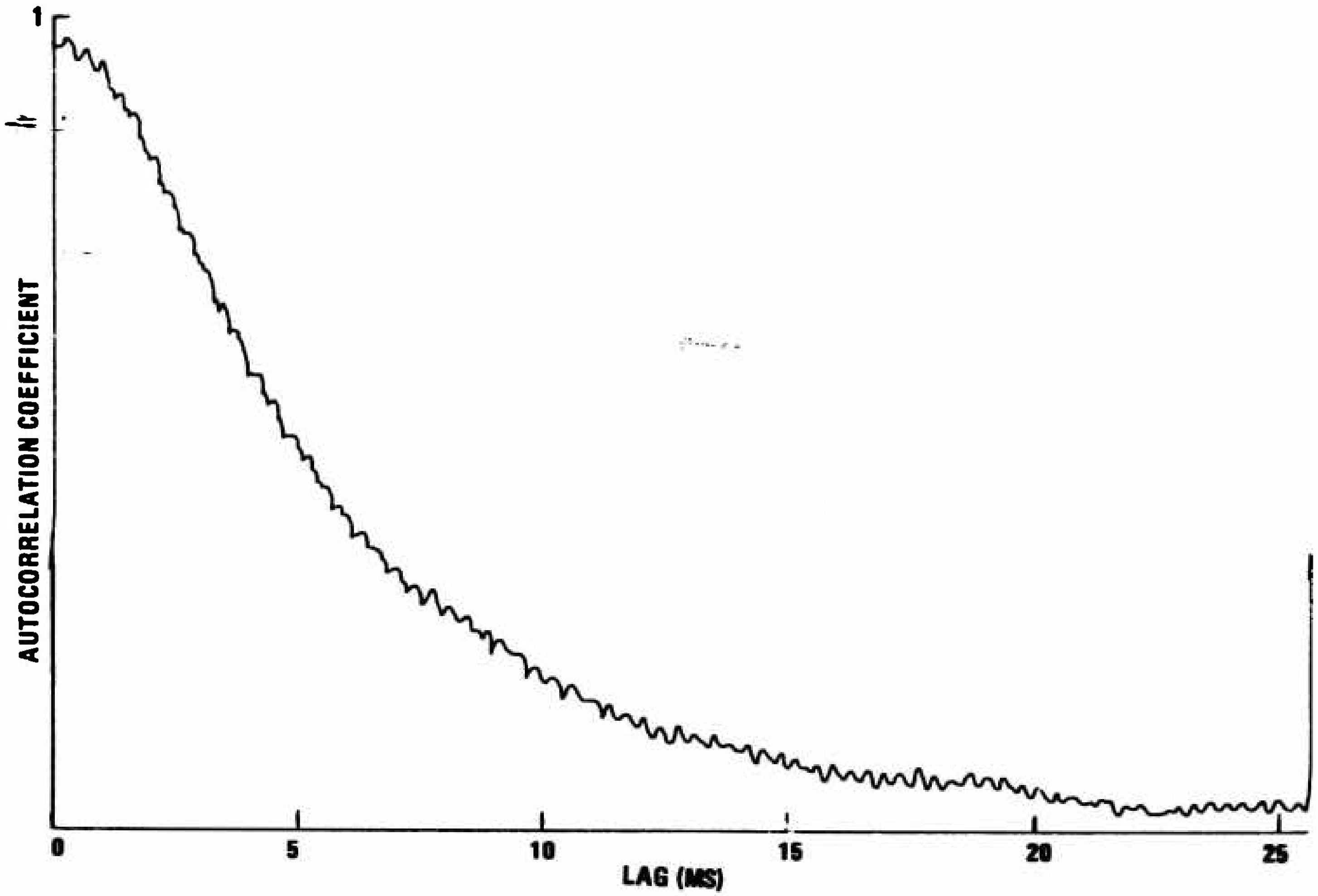

Figure 21. Autocorrelation Coefficient vs. Lag; x-band, 6μs Range Horizontal Polarization, Runs 19-27.

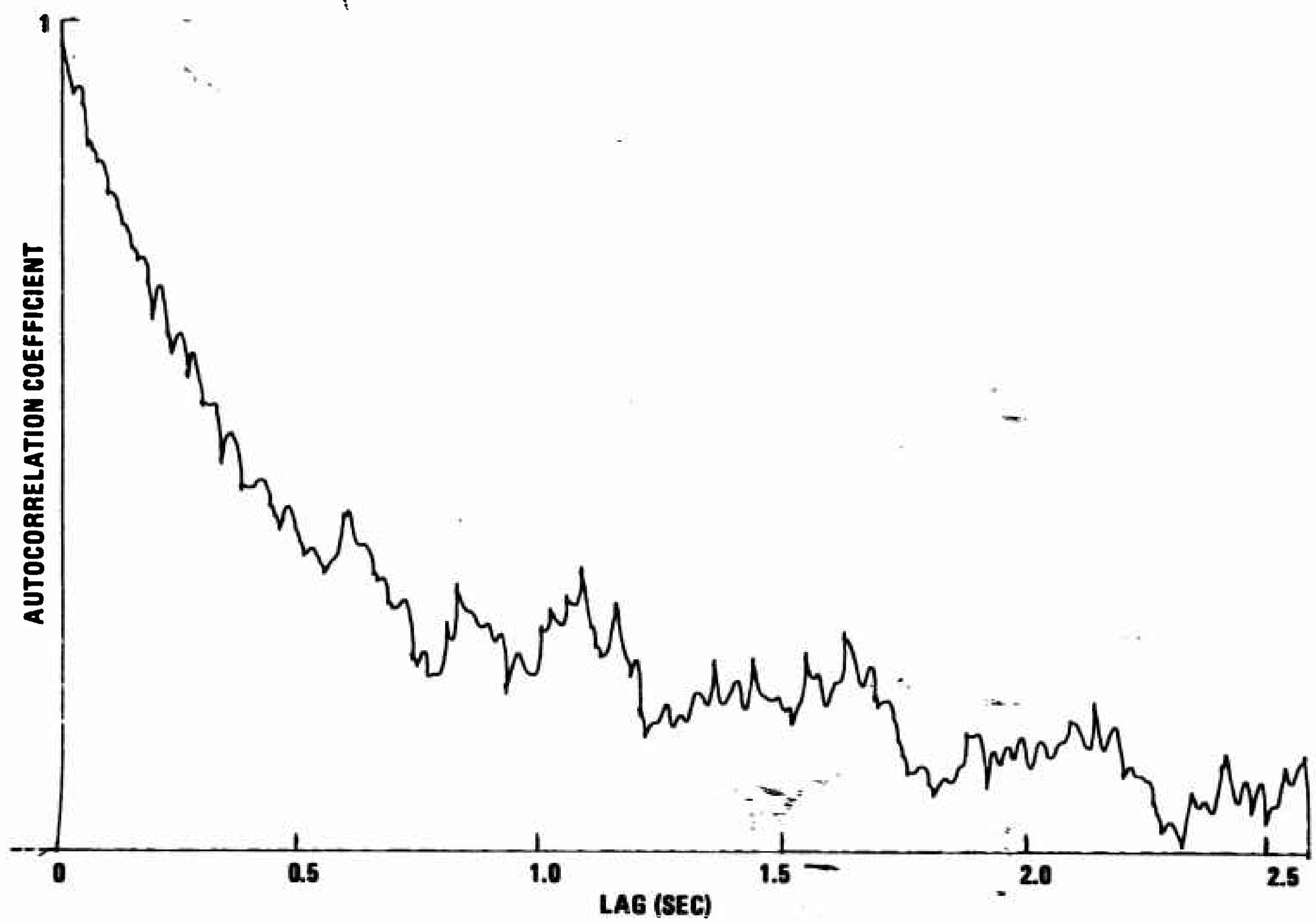

Figure 22. Autocorrelation Coefficient vs. Lag; x-band, 6μs Range Horizontal Polarization, Runs 19-30.

zero, of the autocorrelation coefficient, the cancellation was not precise because of the inevitable lack of stationarity in real clutter data. Thus, the location for the zero value is ambiguous and not assigned here; it is left to the reader to choose a level for his own purposes.

In Figure 19 is seen an estimate of autocorrelation coefficient which was made with lag steps of 100 μs, a smoothing time constant of 400 μs, and a total number of products integrated per lag unit of 4096. Thus, the total lag is 25.6 ms and the data run spanned 105 seconds. The curve is seen to consist of a peak near zero lag of width approximately 1 ms and some cyclic oscillation on the slowly falling (on this time scale) tail. The width of the peak is set partly by the Doppler fluctuation in the video signal and partly by the smoothing filter. It is unfortunate that the radar and instrument parameters are such as to give no good quantitative estimate of the Doppler bandwidth of the sea return at this wavelength. The cyclic oscillation is caused by 400-Hz hum in the 3-mm radar video.

In Figure 20, a longer lag scale has been used to display the decorrelation caused by sea-surface rearrangement (as distinguished from internal Doppler); the width of this decay is of the order of 0.5 sec for the conditions observed. The decay is more a property of the wave motion than of the parameters of the radar, and it has been found to be only weakly tied to radar cell size and to be almost independent of wavelength. The sea state on this date was low and the maximum lag short, so that a feature seen normally in data taken in high-wave conditions is missing; that feature is a cyclic behavior of the curve at the rate of the wave period. In the present instance, signal samples taken about 1 second apart could be considered as uncorrelated. This estimate was made with 10 ms per lag step, 40-ms smoothing time constant, and 512 products summed per lag.

In Figure 21 is shown a short-lag-time estimate of the autocorrelation coefficient for X-band clutter. The Doppler width here is about 5 ms for the conditions observed (a range of 3 to 10 ms is typical). The processor parameters were the same as for Figure 19. The prime-power hum is not visible here partly because the X-band radar is powered from a 60-Hz source.

In Figure 22 is shown a longer lag estimate from X-band video with the same processor parameters as for Figure 20. Again the 0.5-sec decay associated with surface rearrangement is seen, and there is here the suggestion of a 0.5-sec-period oscillation, the cause for which is not obvious.

It should be emphasized that these curves are estimates computed from logarithmic video. If they are to be used for system study in which linear or square-law detectors are postulated, then the methods of Reference 7 must be applied to transform the curves to the appropriate video domain.

IV. CROSS SECTIONS OF TARGETS ON THE SEA

Targets are considered in two groups, those which are small in physical size and of the order of low wave heights and those which have higher profiles. The latter class consists mostly of boats and ships.

A. Small Targets

In Table IV are assembled data from Appendix B on the 3-mm radar cross section of small targets measured on the sea surface. These data are "effective" cross sections, by which is meant that they include the effects of the water surface which supports the targets and are not the intrinsic free-space cross sections of the targets alone. The entries in Tables IV and V are average cross sections from runs of 160-sec length and were computed from the 0.9-cumulative values by subtracting 3.5 dB, as was done for the clutter data.

Some of the targets were deliberately placed on the water and some were incidentally visible. The drums and 4-foot spar buoy marked a dredging operation about a mile away. One swimmer was on vacation, one was a worker. The two spheres were light-weight spun aluminum with unknown tolerances, so that their cross sections certainly had an inherent aspect dependence. The sonobuoys were not active but were mechanically complete and were weighted to float at the correct height.

It can be seen from the table that there is a substantial variation in the data for a given target, so that there are no well-defined trends. However, there does seem to be a difference between the vertical and horizontal cross sections of the targets; it averages 3.9 dB for the data from swimmers, spheres, and sonobuoys. However, this difference might also be associated with other factors peculiar to the conditions because the vertical and horizontal data were not taken on the same days. There also seems to be a reduction in cross section with increasing range. This effect is reasonable because one would expect that shadowing of small targets by wave crests is more complete as range increases. The effect of shadowing was dramatically demonstrated on one day when the average wave height was estimated to be 2.5 feet. The target return densities were bimodal, indicating that the target tended to be either visible or completely shadowed. Figure 23 is a replica of a typical probability density function for such a case. The abscissa is

TABLE IV

3-mm Radar Cross Section of Small Targets

Date-Run	Target	Pol.	Range	σ_t	Std. Dev.
31-36	55 gal. drum	HH	14.0 μs	-13.1 dBsm	5.0 dB
10-2	55 gal. drum	HH	15.0 μs	-12.5 dBsm	---
10-14	55 gal. drum	HH	12.2 μs	-14.6 dBsm	---
10-13	4' Spar buoy	HH	12.1 μs	- 1.5 dBsm	4.9 dB
6-17	Swimmer	VV	1.4 μs	-16.9 dBsm	4.2 dB
6-18	Swimmer	VV	1.4 μs	-15.2 dBsm	4.5 dB
10-21	Swimmer with mask	HH	4.2 μs	-14.8 dBsm	7.4 dB
10-22	Swimmer without mask	HH	4.2 μs	-13.8 dBsm	6.7 dB
11-21	Swimmer without mask	HH	5.6 μs	-13.0 dBsm	5.2 dB
6-22	Small sphere	VV	2.7 μs	-10.8 dBsm	5.0 dB
11-7	6" dia. sphere	HH	4.0 μs	-12.2 dBsm	7.0 dB
11-14	6" dia. sphere	HH	5.6 μs	-18.4 dBsm	6.5 dB
6-28	12" dia. sphere	VV	2.0 μs	- 8.6 dBsm	3.7 dB
18-6	12' dia. sphere	VV	4.4 μs	-12.4 dBsm	6.8 dB
13-17	12' dia. sphere	VV	7.0 μs	- 7.7 dBsm	4.5 dB
11-8	12" dia. sphere	HH	4.0 μs	+ 0.7 dBsm	6.5 dB
11-15	12" dia. sphere	HH	5.6 μs	- 5.9 dBsm	6.3 dB
11-22	12" dia. sphere	HH	9.0 μs	-11.6 dBsm	6.5 dB
18-4	AN/SSQ-41 sonobuoy (#2)	VV	4.35μs	-13.4 dBsm	6.5 dB
11-23	AN/SSQ-41 sonobuoy (#2)	VV	9.0 μs	-19.1 dBsm	---
11-9	AN/SSQ-41 sonobuoy (#2)	HH	4.0 μs	- 6.7 dBsm	7.8 dB
11-16	AN/SSQ-41 sonobuoy (#2)	HH	5.6 μs	- 7.8 dBsm	7.5 dB
6-34	AN/SSQ-49 sonobuoy (#4)	VV	3.0 μs	-11.1 dBsm	9.2 dB
11-12	AN/SSQ-49 sonobuoy (#4)	HH	4.0 μs	- 0.1 dBsm	11.1 dB
11-19	AN/SSQ-49 sonobuoy (#4)	HH	5.6 μs	- 5.1 dBsm	8.0 dB
6-35	AN/SSQ-50 sonobuoy (#12)	VV	3.0 μs	- 9.5 dBsm	6.5 dB
13-30	AN/SSQ-50 sonobuoy (#12)	VV	7.0 μs	- 9.2 dBsm	---
11-11	AN/SSQ-50 sonobuoy (#12)	HH	4.0 μs	- 1.4 dBsm	10.0 dB
11-18	AN/SSQ-50 sonobuoy (#12)	HH	5.6 μs	- 8.3 dBsm	7.4 dB

TABLE V

3-mm Radar Cross Section of Boats

Date-Run	Target	Aspect	Pol.	Range	σ'_t	Std. Dev.
5-9	25' fishing boat, with tower	Qtr.	VV	11.4μs	+11.0 dBsm	5.2 dB
5-10	20' fishing boat	--	VV	16.8μs	+16.0 dBsm	6.1 dB
5-11	15' boat, outboard	Qtr.	VV	15.5μs	+ 1.9 dBsm	4.4 dB
5-12	25' fishing boat, high cabin	Stern	VV	15.5μs	+ 9.7 dBsm	4.5 dB
6-24	10' fiberglass with 2 men and outboard	Broadside	VV	2.5μs	- 3.5 dBsm	5.4 dB
6-36	10' fiberglass with 2 men and outboard	Broadside	VV	2.5μs	- 0.5 dBsm	5.4 dB
6-37	10' fiberglass with 2 men and outboard	Qtr.	VV	2.8μs	- 4.9 dBsm	4.5 dB
6-38	10' fiberglass with 2 men and outboard	Stem	VV	3.5μs	+ 0.1 dBsm	5.0 dB
6-39	10' fiberglass with 2 men and outboard	Off-bow	VV	3.4μs	- 3.0 dBsm	4.2 dB
6-40	10' fiberglass with 2 men and outboard	Bow	VV	2.5μs	- 6.0 dBsm	3.9 dB
12-1	10' fiberglass with 2 men and outboard		VV	5.6μs	- 7.5 dBsm	5.5 dB
13-5	10' fiberglass with 2 men and outboard		VV	5.6μs	+ 2.6 dBsm	6.2 dB
10-11	15' open outboard	Qtr.	HH	12.5μs	+ 1.6 dBsm	5.0 dB
10-12	25' to 30' fishing boat	Qtr.	HH	11.9μs	+14.7 dBsm	5.2 dB
10-15	20' inboard	Stern	HH	15.4μs	+12.8 dBsm	7.5 dB
10-16	20' sailboat		HH	19 μs	+ 5.8 dBsm	4.5 dB
10-17	20' sailboat		HH	17 μs	+ 1.4 dBsm	5.9 dB
10-10	Ship, unidentified	Near Broadside	HH	74 μs	+16.0 dBsm	---

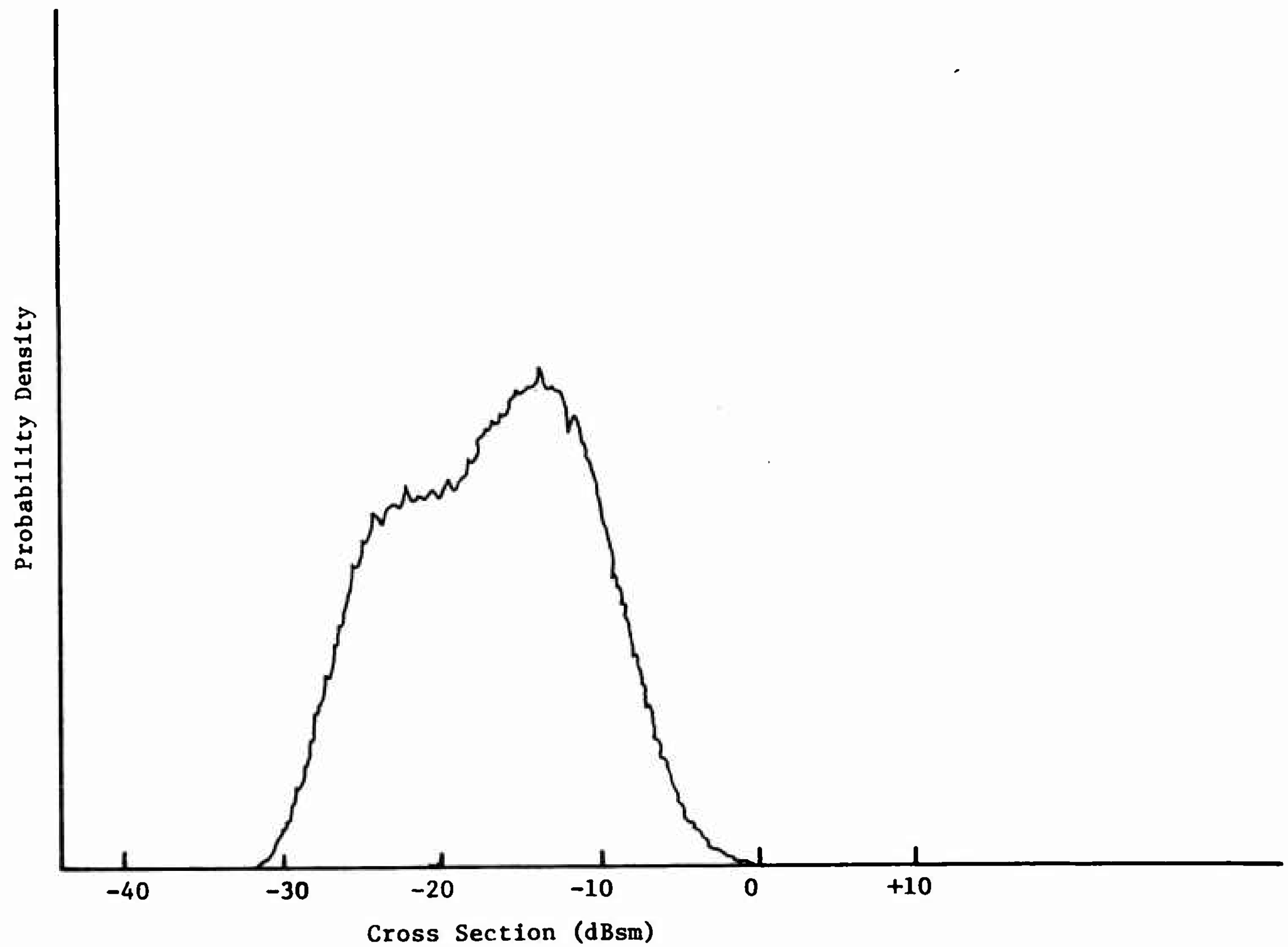

Figure 23. Probability density of cross section for a 12-inch sphere in a high sea (18 Aug., run 6)

calibrated in dBsm but the ordinate is uncalibrated. A measure of width of the distributions of returns is shown in the last column of Table IV. It is seen that the fluctuation of sonobuoys covers more dynamic range than simpler targets.

B. Boats

Boat cross-section data are assembled in Table V. The small 10-foot fiberglass boat was under control, whereas all the others were targets of opportunity. The fiberglass boat was operated with 2 men aboard and a small (5 h.p.) outboard motor. The freeboard when so loaded was about 8 inches and the seats were about 4 inches above the waterline. There was no metal visible in the boat except for the motor. The data shown were taken at minimum speed. The cross section is seen to behave with aspect variation much as boat cross sections do at lower frequencies. The broadside and stern aspects have large return and bow and quarter aspects show low return. For the larger craft the smallest average cross section was +1.4 dBsm and the largest +16 dBsm.

V. DISCUSSION

In this chapter are collected comments of interpretation of the data presented in Chapters III and IV.

A. Accuracy and Variability of the Data

The accuracy of the data presented is influenced by the errors in assigned values of cross section of the standard corner reflector and readings of the precision attenuator, as well as by the variability of the attenuator setting, the radar system power and gain, the data-reduction steps and the inherent fluctuation of the process being observed. At the beginning of the experiment period the variation of radar gain and power was on the order of ± 4 dB, but in the last half of the period the variation could be held to less than ± 1 dB. The largest contributors to this improvement were changes in antenna-aiming and receiver-tuning procedures. The pedestal was rearranged so that the operator's movements near the radar did not affect the aiming, and the receiver was tuned immediately before each data run so long-term drift was reduced. Short-term changes in gain and video offset were reduced to less than ± 0.5 dB, and long term (over a period of a few days) to about ± 1 dB. The variability inherent in the signals from clutter and targets on the sea was substantially greater than these levels, although under some conditions adjacent 160-sec runs repeated to within ± 1 dB (see Figure 13 for example). Other than the manufacturer's experience, there is no calibration information available on the precision attenuator. Its resetability appeared to be less than 0.5 dB.

The cross section of the corner reflector was calculated from a formula based on geometric optics. The size of the corner is such that resonance effects are not likely to be troublesome (e.g., $a/\lambda \simeq 23$). The accuracy of the corner is not known, but the fabrication process appeared to retain the inherent flatness of the basic material and the accuracy of the machine on which the 90° angles were established. If the corner were imperfect the result would be most a reduction of its cross section, thus causing all of the cross section values of this report to be higher than correct. Therefore, the numbers reported here may be considered an upper bound to the correct values except for the variability of the estimates.

As was described in Chapter II, the average received power was estimated from the power corresponding to 0.9 cumulative probability. The number relating the two levels (3.5 dB) was established by numerically integrating a moderate number of previously observed and carefully measured clutter and target distributions; it has been found to hold within $\pm$ 0.5 dB under the variations of the detailed shape of the distributions. This does not imply that no distributions will be measured in the future which do not conform to this rule, but the shapes of the distributions of data reported here do qualify for its use.

The aggregate of variability introduced by the data acquisition and reduction process was such that variations observed can be considered to be significant for the most part, especially if obtained in the latter half of the period. By significant is meant that the variation was inherent in the scattering process and is not an artifact introduced by an imperfect measuring system. Subject to a couple of important assumptions, the σ° values are believed to be accurate within about ± 2 dB, whereas the values of target cross section are probably underestimated because of difficulties of tracking in both range and antenna aiming angles.

B. Comparison of Vertical and Horizontal Returns at 3 mm

A most striking result of the experiments is that σ° for vertical polarization is substantially less than that for horizontal polarization. This result is in sharp contrast to data obtained at lower frequencies, especially for nearly smooth sea surfaces where σ° for vertical polarization is much larger than for horizontal. This result is interpreted by noting that the ratio $\sigma^\circ_{VV}/\sigma^\circ_{HH}$ is determined by two phenomena which are manifestations of the same physical property of the water surface, namely its complex permittivity. The dielectric constant of the water determines the reflection coefficient for forward scattering and also the absorption coefficient. A high reflection coefficient (near unity) produces cancellation at the surface between direct and surface-reflected waves, because there is a phase change of about 180 degrees for near-grazing incidence. A high absorption coefficient (near unity) would be expected to make the surface transparent or non-reflecting for backscatter as well as for forward scatter.

When the surface is rough, substantial phase spread can be introduced into the surface-reflected wave so that the amplitude of the coherent or plane-phase component, is reduced below its smooth-surface value. Thus, the effective reflection coefficient for forward scattering is the product of the Fresnel reflection coefficient, ρ_f, and a roughness factor, ρ_r.

The backscattered energy may be considered to be a function of at least three factors: a roughness factor which causes the scattering, an illumination factor determined by interference, and an effective dielectric reflection factor. The first and second are certainly monotonic increasing functions of roughness, and both tend to saturate [8, 9]. Assume that a surface is rough enough so that no interference effect is present. Then one might estimate the effective dielectric reflection factor from

$$\bar{\rho} = \frac{\int_0^\infty \rho(\varepsilon,\psi)\exp(q^2/2q_o^2)dq}{\int_0^\infty \exp(q^2/2q_o^2)dq} \qquad (13)$$

where $\rho(\varepsilon,\psi)$ is the Fresnel reflection coefficient [10] for complex dielectric constant ε and incidence angle ψ, and the Gaussian factor is a weighting function of surface slopes, $q = \tan\psi$ [11]. Carrying out the integrals in Equation 13 for $\varepsilon = 4.93 - j1.42$ [12], and $q_o = 0.3$ one finds that $\bar{\rho}_{HH} = 0.83$, and $\bar{\rho}_{VV} = 0.43$, so that on the basis of dielectric reflection alone $\sigma°_{VV}/\sigma°_{HH}$ is predicted to be -5.7 dB in the absence of interference effects. This is to be compared with the measured average value of -4.8 dB.

A tentative conclusion drawn from the above arguments is that at 3-mm wavelength such interference effects as exist are weak in the angle regime observed. This conclusion is also supported by the weak range dependence, on the order ψ^0 to ψ^{-1} in many runs, which would be much steeper if substantial interference effects were present. The fall-off as ψ^{-1} at the higher wind speeds observed is tentatively interpreted as due to shadowing. The decrease in $\sigma°$ at low sea states with decreasing range (increasing angle) is possibly due in part to the reduction in dielectric reflection at higher angles. This effect is not sufficient alone to explain the observed decrease in σ° of about 5 dB for low seas and high angles (5 deg.) because the total change from grazing to vertical incidence is expected to be only 8 dB for horizontal polarization.

C. σ° at 3-mm

The values of σ° observed here compare comfortably with the bulk of previous experience [e.g., 2, 3 and 4], but are somewhat lower than the values observed in one instance [13]. In the latter experiment, σ° values between -20 and -34 dB were reported at an incidence angle of 1.4 degrees. Although polarization was not mentioned in that report, these values are perhaps 10 dB higher than those of the present report. It is interesting to note that the occurrence of σ° decreasing with range observed in the present experiment for cross-wind or low-sea-state conditions is in agreement with one observation of Reference 13 which was associated with looking parallel to the swell crests.

D. σ° at X-band

It should be acknowledged that some of the σ° values in Figure 12 for X-band clutter are somewhat higher than given values which are generally published. Sufficient effort was devoted to assure that obvious errors or calibration problems were not responsible for these high observed values. For the same incidence angles and an assigned sea state number of 2.5 the tables of Reference 2 imply an expected value of σ° near -40 dB, which is of the order of 20 dB below that observed here. The presented data are generally for upwind observations whereas the data of Reference 2 are averaged over all aspect angles. However, this averaging could expect to lower σ° only about 6 dB below upwind values at X-band. Such anomalies as this appear occasionally in reported experiments, but no clear explanation is offered. The compilation in Reference 2 and the majority of the data from which it was drawn imply that such high σ° values as these are felt to be of low frequency of incidence. Until a more complete understanding of the conditions under which high values are observed is available the attitude which labels these occurrences as anomalies can be dangerous.

E. Noise-Limited Detection with Millimeter Radar

During the experiment period, the receiver noise output corresponded to an average received signal about 48 dB below that received from the standard corner reflector at a range of 2240 feet. If the parameters from Table I are used with the free-space radar equation, an effective noise figure for the radar can be calculated. Assume nominal parameters of

$$
\begin{aligned}
P_t &= 4 \text{ kW} \\
G &= 53 \text{ dB} \\
\lambda &= 3.16 \text{ mm} \\
\sigma_t &= 11 \text{ m}^2 \\
R &= 683 \text{ m} \\
L &= 7.9 \text{ dB (5.5 dB for duplexer, 2.4 dB for waveguide).}
\end{aligned}
$$

Then a received peak power of -70 dBm is calculated to be equal to receiver noise. Thermal noise in a bandwidth of 40 MHz corresponds to -98 dBm, so that an effective noise figure of 28 dB is inferred. This number includes the actual noise figure plus the departure of the above parameters from their nominal assumed values plus any other losses not included. No clue is available as to the correct assignment of contributions to this figure.

The above noise figure appears excessive and probably can be reduced with effort to no greater than 18 dB. Assume that this is done so that an estimate of maximum detectable range can be made. Using a criterion of minimum detectable target-signal-to-noise ratio of +5 dB* for typical intensity-modulated display one predicts a maximum range for detection of 14 km for a +10 dBsm target typical of larger boats and 4.5 km for sonobuoys (-10 dBsm considered average at longer ranges). Without the above-cited reduction in noise figure these ranges would be reduced to the order of 7.8 and 2.5 km, respectively.

F. Clutter-Limited Detection

Although extensive calculations for prediction of target detection in a clutter background are inappropriate here, some comments should be made. It was the experience of these observations that returns from sono-

*It may not be possible to realize this criterion if short dwell time on target is required for large-area-search coverage.

buoys (the smallest targets measured) were adequate for detection in all of the conditions that were met. One instance, in which one sonobuoy was visible and one was not, serves to define one point on the envelope of marginal detection. This point is defined by the parameter set:

Range	4.4 μs
Angle	1.9 deg.
Wave height (h_{av})	2.5 ft.
Wind speed	9.5 kts
Look direction	Upwind
Polarization	VV
Measured $\sigma°$	-36 dB

Other radar parameters were the same as those in Table I. For these data, the area of the cell was +15.7 dBsm and the average clutter cross section was about -20 dBsm. The measured cross section on the sonobuoy that could be seen well enough to be tracked was -13 dBsm, making the target-signal-to-clutter ratio about 7 dB. It should be noted that the sea was high, with swell dominating the wave structure, so that detection was hampered by the low profile of the target, the low incidence angle and the upwind and upwave look direction.

VI. ACKNOWLEDGEMENTS

The 3-mm radar was provided by the Naval Air Development Center, Johnsville, Pennsylvania, and was operated by Mr. Marvin Foral, assisted by Mr. Leo Marella of that facility.

The data were recorded by the author, assisted by Messrs. Steven Zehner, Clark Butterworth, and Cliff Burdett of Georgia Tech. The X-band radar and field site were utilized with the kind permission of Ships Engineering Center, U.S. Navy Bureau of Ships.

Respectfully submitted,

F. B. Dyer
Project Director

Approved:

R. M. Goodman, Jr.
Head, Sensor Systems Branch

VII. REFERENCES

1. D. E. Kerr, Ed., Propagation of Short Radio Waves, McGraw-Hill (1957); Sec. 6.6.

2. F. E. Nathanson, Radar Design Principles, McGraw-Hill (1969); Chap. 7.

3. C. R. Grant and B. S. Yaplee, "Backscattering from Water and Land at Centimeter and Millimeter Wavelengths," Proceedings of the IRE 45 976 (Jul 1957).

4. J. C. Wiltse, S. P. Schlesinger, and C. M. Johnson, "Backscattering Characteristics of the Sea in the Region from 10 to 50 KMC," Proceedings of the IRE 45 220 (Feb 1957).

5. M. Skolnik, Introduction to Radar Systems, McGraw-Hill (1964); Chap. 11.

6. D. K. Barton, Radar System Analysis, Prentice-Hall (1964); Sec. 3.5.

7. G. E. Uhlenbeck, Radiation Laboratory Report No. 454 (15 Oct 1943); see also Ref. 1.

8. J. C. Daley, W. T. Davis, and N. R. Mills, "Radar Sea Return in High Sea States," NRL Report 7142 (25 Sep 1970).

9. C. I. Beard, I. Katz, and L. M. Spetner, "Phenomenological Vector Model of Microwave Reflection from the Ocean," IRE Trans AP-4 162 (Apr 1959).

10. J. A. Stratton, Electromagnetic Theory, McGraw-Hill (1941); Sec. 9.5.

11. B. Kinsman, Wind Waves, Prentice-Hall (1964).

12. J. A. Saxton and J. A. Lane, "Electrical Properties of Sea Water," Wireless Engineer 29 269 (Oct 1952).

13. C. W. Tolbert, C. O. Britt, and A. W. Straiton, "Back Scattering Cross-Sections at 4.3-mm Wavelengths of Moderate Sea Surfaces," Report No. 95, E.E.R.L., U. of Texas (8 Nov 1957).

14. W. K. Rivers, S. P. Zehner, and F. B. Dyer, "Modeling for Radar Detection (U)", Final Report Contract N00024-69-C-5430, Georgia Institute of Technology, (31 Dec 1969), Secret.

15. J. Aitchison and J.A.C. Brown, The Lognormal Distribution, Cambridge University Press (1966); Section 2.3.

16. D. R. Cox, Renewal Theory, Methuen (1962); Section 1.4.

17. M. Katzin, "On the Mechanisms of Radar Sea Clutter," Proceedings of the IRF 45 (1957).

18. J. V. Harrington, "An Analysis of the Detection of Repeated Signals in Noise by Binary Integration," IRE Transactions on Information Theory 1 1 (1955).

VIII. APPENDICES

A. A Statistic of Radar Sea Return*

Abstract. The video level corresponding to average radar sea-clutter power appears to lie 3.5 ± 0.5 dB below the 0.9 cumulative probability level independent of the detailed shape of the distribution.

Detection of radar target signals in a background of sea clutter requires a larger target return than detection in a background of receiver noise having the same average power as the clutter. In part this is because the dynamic range of sea-return signals is greater than that of receiver noise signals, which are inherently Rayleigh distributed. The probability distribution is variable, and its width depends on such factors as polarization, radar cell size, sea state, and grazing angle of incidence. This variability seriously affects the accuracy of estimates of average received clutter power, which is the principal measured quantity in studies of the deterministic behavior as a function of such variables as wavelength, wind speed, wave height, incidence angle, and the angle between wind vector and antenna boresight.

A method often used in the past to estimate the average received power has been to average the video output of a radar receiver. If the envelope (video) detector is a square-law device, such an average of the video signal represents the average received power. However, the transfer characteristic of the square-law detector places stringent requirements either on the dynamic range of the averager or on the gain setting ahead of the envelope detector, or both. Dynamic range requirements after the detector are reduced if a "linear" rectifier is used, but correction factors are required when signals of variable distribution are observed. In addition, the effects of video-detector threshold and amplifier saturation associated with real receivers will limit dynamic range and affect the accuracy of average-power estimates for signals with large dynamic range. The requirements for large dynamic range for estimating the average received power can be reduced by the use of a property of probability distributions of typical clutter

*This section summarizes unpublished material generated under Contracts N00024-69-C-5430 and N00024-70-C-1219.

signals which relates the average received power to a unique point on the distribution.

It was noticed that a unique relationship existed among cumulative probability distributions of clutter signals calculated [14] from physical models for the sea surface and propagation near it. The models are based on a Gaussian height-distributed water surface illuminated by a forward-scattered interference field [9]. One set of the calculated curves is reproduced in Figure 24, in which cumulative probability $P(v<v^*)$ is plotted on normal probability paper against the receiver video threshold, v^*, for a logarithmic video detector. The parameter, r_U, of the family is the ratio of radar cell dimension to the horizontal decorrelation distance of the sea-surface height. The curves are normalized such that all correspond to the same average received power: -9.3 dB on the abscissa. It is apparent that the curves cross near a point which occurs at about 0.9 cumulative probability for every curve. Thus the average power corresponds in this case to a point about 3.5 dB below the 0.9 cumulative video level.

The same property cited above is shared by two other families of distributions in current usage to represent radar clutter echoes, the log-normal and Weibull cases. The log-normal family is described by a set of straight lines in the graphical form chosen for Figure 25, normal probability paper and a logarithmic video scale. The log-normal curves plotted in Figure 25 all have the same average power (0 dB), which is related to their medians by [15]

$$\rho(\mathrm{dB}) = \frac{\ln 10}{20} \; \sigma_\ell^{\,2}(\mathrm{dB}), \tag{14}$$

where $\rho(\mathrm{dB})$ is the mean-to-median ratio in dB and $\sigma_\ell(\mathrm{dB})$ is the standard deviation of the distribution in dB. The Weibull family is represented by [16]

$$P(v<v^*) = 1 - \exp\{-[\Gamma(1 + \tfrac{1}{b})]^{b} \exp[\tfrac{b\ln 10}{10} v^*]\} , \tag{15}$$

and is plotted in Figure 26 for values of the parameter b shown and constant average power of 0 dB. It is seen that the log-normal set for 3 dB $\leq \sigma_\ell \leq$ 8 dB cross at video levels

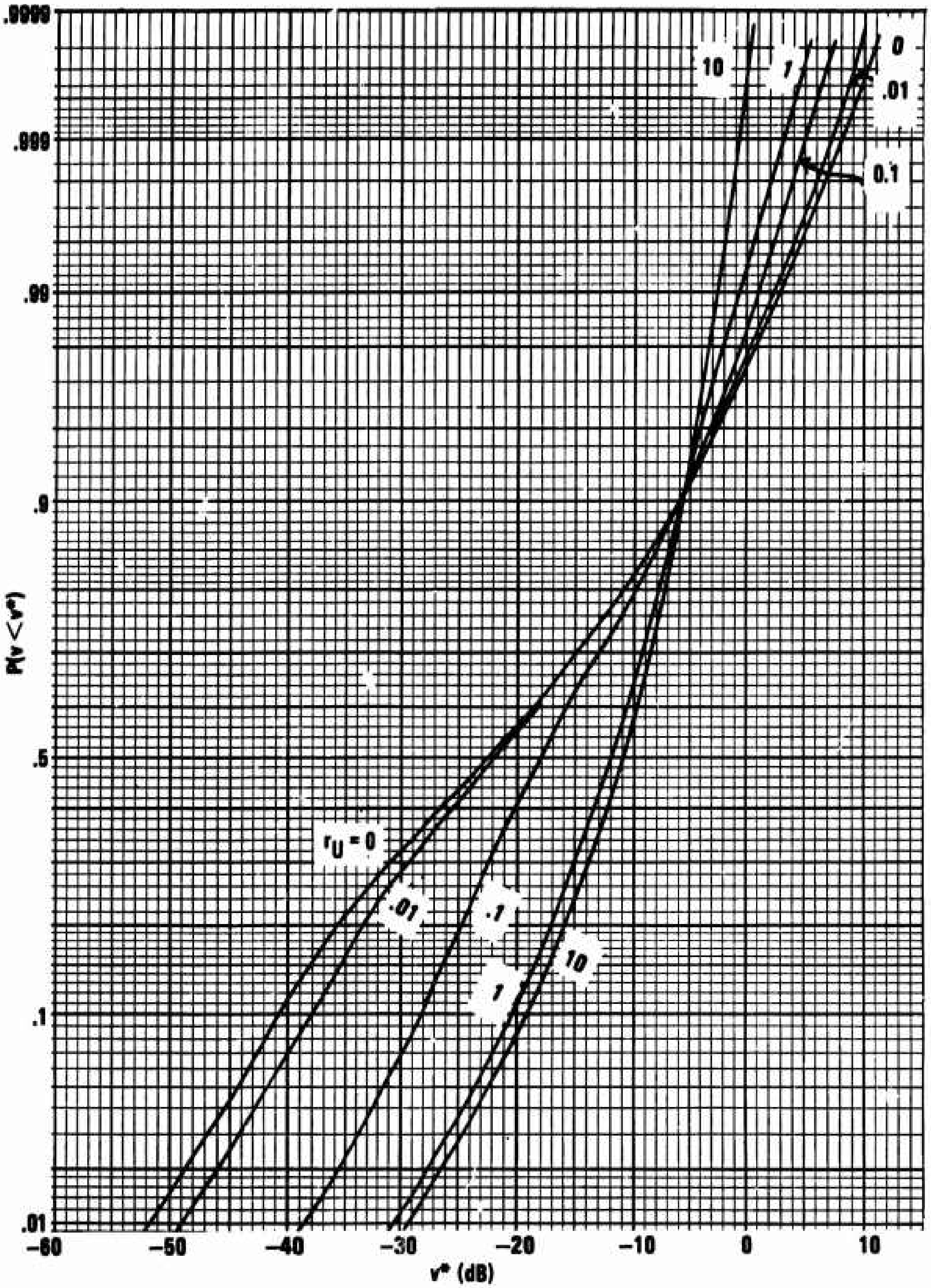

Figure 24. Calculated Cumulative Distributions of Sea Return.

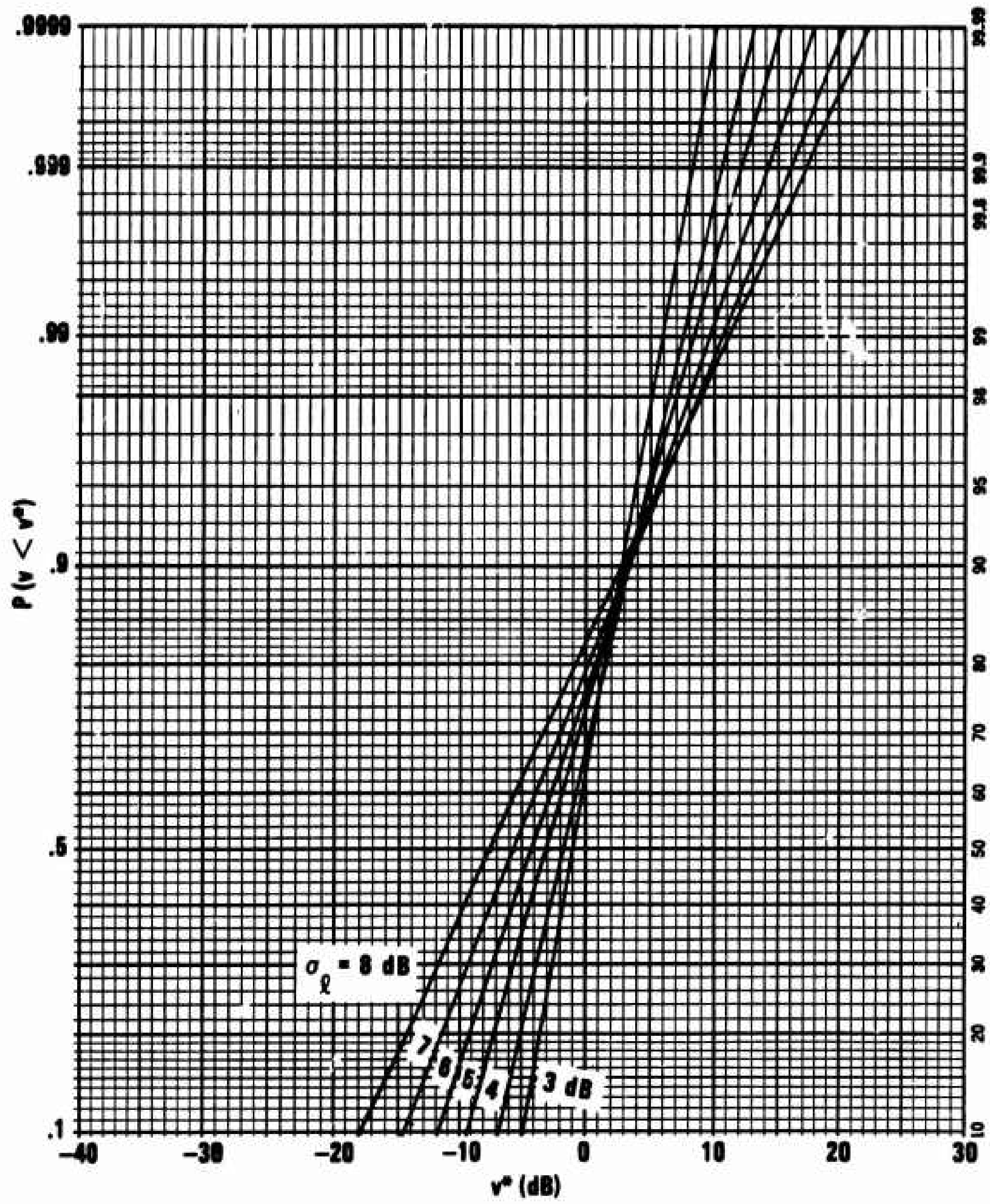

Figure 25. Log-normal Cumulative Distributions.

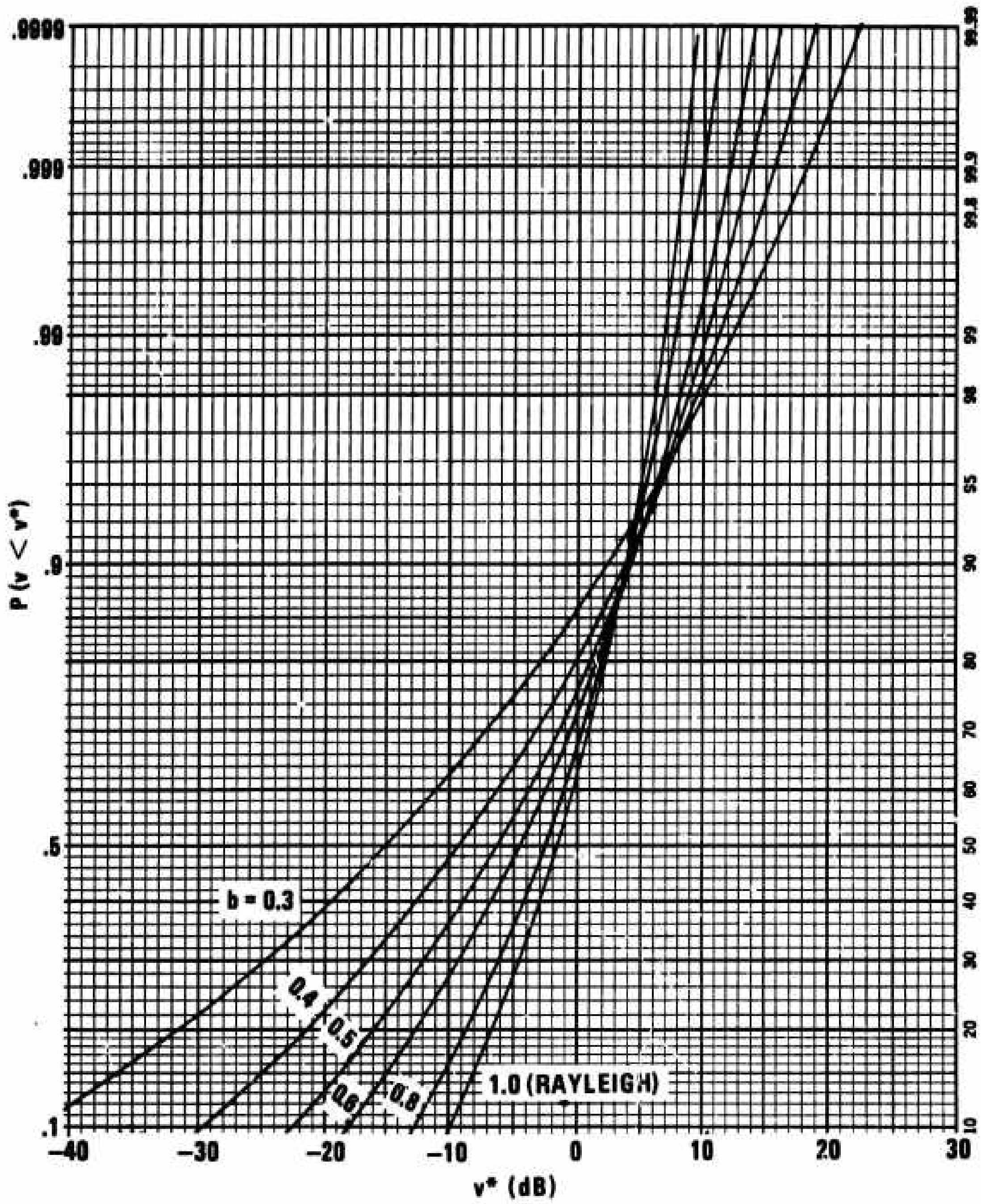

Figure 26. Weibull Cumulative Distributions.

about 3.2 dB above their average, and the Weibull for $0.4 \leq b \leq 1$ at about 4.0 dB above their average. It should be noted that the Rayleigh distribution, which describes receiver noise, is a member of the Weibull family (b = 1.0).

For the three families of distributions shown, it is concluded that their average powers correspond to points lying 3.5 ± 0.5 dB below the video level corresponding to 0.9 cumulative probability (of the video being below that level). This relationship has been found to hold for distributions of signals recorded from real clutter returns. In Figure 27 are plotted such distributions for two transmitted polarizations. The pertinent radar parameters are shown in Table VI.

Table VI

Radar Parameters for Clutter Data of Figure 27.

Frequency	9400 MHz
Pulse Length	0.2 μs
Azimuth Beamwidth	0.8 deg
Antenna Height	75 feet
Range	3 nmi
Look Direction	Upwind
Wind Speed	17 knots
Average Wave Height	2.5 feet
Sample Size	5 min at 4 kHz

The abscissa corresponds to cross-section per unit cell area expressed in dB with respect to 1 square meter. The range indicated is slightly beyond the transition point dividing the R^{-3} and R^{-7} regions of range dependence of returned clutter power [17].

It is seen that the dynamic range for horizontal polarization is greater than for vertical, and that its average is higher. The average cross-sections were calculated numerically from the curves using the relationship

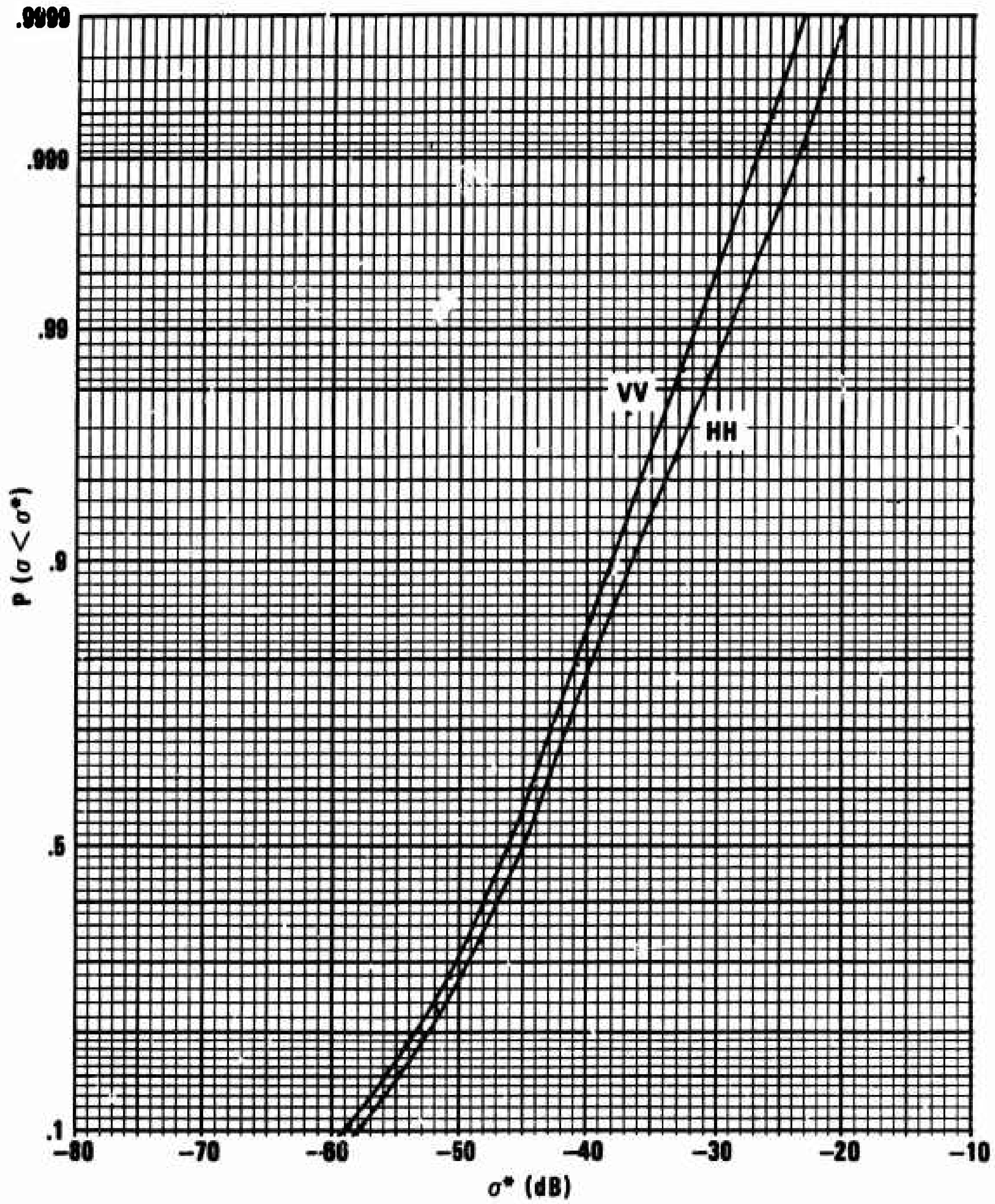

Figure 27. Experimental Cumulative Distributions; x-band.

$$\sigma^\circ = 10 \log \int_0^1 \exp \{\frac{\ln 10}{10} \sigma^*\} \, dP \quad , \tag{16}$$

where P is the ordinate variable, cumulative probability. The average cross-sections per unit area, σ°, were found to lie 3.3 and 3.6 dB below their 0.9 cumulative probability levels for horizontal and vertical polarizations, respectively.

It is suggested by this limited set of comparisons that a useful property exists relating the average received power of radar sea clutter and the 0.9 cumulative probability level. This property should find utility when only an estimate of the average power of a signal is of interest, as well as in specification of distribution-free detection systems of double-threshold type [18].

B. Cross Section and σ° Data

Table VII presents a summary of cross section and σ° values calculated from the measured distributions and accompanying calibration runs. It is from this data set that the analyses of Chapters III and IV were extracted. The original data were recorded in the format of Figures 5, 6, and 28; the last is a copy of the form used as a guide in recording the data supporting the signal distributions.

In Table VII, the wind speed is given in knots, followed by the upwind bearing in degrees magnetic and the average wave height in feet. The look direction of the radar is also given in degrees magnetic. The range is given in microseconds of 2-way time-of-flight (1 μs corresponds to ≃ 150 m range). For clutter, the tabulated value is σ°, the average cross section per unit area, in dB, calculated according to the procedure described in Chapter II. For targets, the tabulated value is cross section in dBsm. The values of σ' and σ° are quoted to the nearest 0.1 dB to reduce the effect of round-off in handling the data. However, the last digit is considered to be insignificant compared to the accuracy and variability of the data.

TABLE VII

Summary of Cross Section and $\sigma°$ Data

Date	Run	Time	Wind Sp/Dir	h_{av}	Look	Band	Pol	Range	Target	σ' or $\sigma°$
31 Jul	31	1555	8.5/135		135	3mm	HH	12.4	Clutter	In noise
1970	32	1558						6.2		-36.9
	33	1601						3.1		-32.4
	36	1620						14.0	Drum Buoy	-13.1
3 Aug	14	1023			150	3mm	HH	6.2	Clutter	-37.2
	15							9.0		-33.8
	16	1028						2.8		-41.6
	17	1035			150	X	HH	6.2	Clutter	-32.5
	19							9.0		-33.3
	20	1048						12.4		-52.3
	23	1102			165	3mm	HH	6.2	Clutter	-36.2
	24				095					-35.2
	25				130					-37.2
	26	1112			145					-33.2
	28	1126			145	X	HH	6.2	Clutter	-37.0
	29				095					-42.0
	30				130					-41.0
	31	1136			165					-35.0
	35	1356			120	3mm	HH	6.2	Clutter	-42.2
	36	1358								-36.2
	37	1412					VV			-42.2

TABLE VII (Continued)

Summary of Cross Section and σ° Data

Date	Run	Time	Wind Sp/Dir	h_{av}	Look	Band	Pol	Range	Target	σ' or σ°
	42	1439			120	3mm	VV	6.0	Clutter	-39.7
	43	1452					HH			-39.7
	45	1455			120	X	HH	6.0	Clutter	-36.8
	46						VV			-33.8
	53	1542			120	3mm	HH	6.2	Clutter	-34.4
	54	1548						6.0		-39.8
	55	1615					VV	6.1		-47.0
	60	1642			120	X	VV	6.2	Clutter	-45.8
	61									-41.5
	62						HH			-38.0
4 Aug	2	1408	6/150	0.5	150	X	VV	6.2	Clutter	-40.5
	6	1420			090	3mm	VV	6.2	Clutter	-44.0
	10	1447			090	X	VV	6.2	Clutter	-40.0
	13	1503					HH			-50.5
5 Aug	7	1447	8.5/040	0.8	090	3mm	VV	6.0	Clutter	-40.4
	8	1457			130					-43.3

TABLE VII (Continued)

Summary of Cross Section and $\sigma°$ Data

Date	Run	Time	Wind Sp/Dir	h_{av}	Look	Band	Pol	Range	Target	σ' or $\sigma°$
	9	1504			135	3mm	VV	11.4	25' Fishing Boat with Tower	+11.0
	10							16.8	20' Fishing Boat	+16.0
	11							15.5	15' Outboard	+ 1.9
	12	1517						15.5	25' Fishing Boat	+ 9.7
	17	1527	6/090		090	X	VV	6.0	Clutter	-47.3
6 Aug	17	1137	<4	.5	180	3mm	VV	1.4	Swimmer	-16.9
	18	1138								-15.2
	22	1446			090	3mm	VV	2.7	6" Al. Sphere	-10.8
	23							2.7	Clutter	-41.2
	24	1452						2.5	10' Fiberglass Boat	- 3.5
	28	1508			090	3mm	VV	2.0	12" Al. Sphere	- 8.6
	29	1511							Clutter	-45.5
	34	1537			090	3mm	VV	3.0	AN/SSQ-49 Sono	-11.1
	35							3.0	An/SSq-50 Sono	- 9.5
	36							2.5	10' Boat-broad	- 0.5
	37							2.8	Qtr.	- 4.9
	38							3.5	Stern	+ 0.1
	39							3.4	Off Bow	- 3.0
	40	1602						2.5	Bow	- 6.0

TABLE VII (Continued)

Summary of Cross Section and σ° Data

Date	Run	Time	Wind Sp/Dir	h_{av}	Look	Band	Pol	Range	Target	σ' or σ°
	45	1623	7/135		090	3mm	VV	4.2	Clutter	-44.7
	46							3.0		-43.7
	47							1.6		-49.9
	48							6.2		-43.9
	49	1434	8.5/135		135	3mm	VV	6.2	Clutter	-37.5
	50							4.3		-36.6
	51							2.9		-36.4
	52							1.7		-38.3
	53	1645						12.4		-37.7
7 Aug	1	0845	4/135	0.6	135	X	VV	6.2	Clutter	-35.0
	2							12.4		-42.3
	3	0853						24.8		-48.2
	5	0903			135	X	HH	6.2	Clutter	-42.0
	6							12.4		-45.3
	7	0910						24.8		-58.2
	16	0956			135	3mm	VV	3.2	Clutter	-49.5
	17	0959						6.2		-42.6
	19	1040			135	3mm	HH	6.2	Clutter	-38.4
	20							3.1		-45.7
	21	1048	4/var.					4.5		-37.0
	22	1310	11/150	.8		X	HH	6.2	Clutter	-22.0

TABLE VII (Continued)

Summary of Cross Section and σ° Data

Date	Run	Time	Wind Sp/Dir	h_{av}	Look	Band	Pol	Range	Target	σ or σ°
	28	1332	12.5/150		090	3mm	HH	3.1	Clutter	-33.6
	29							4.5		-35.1
	30							6.2		-36.1
	31							9.3		-38.0
	32	1347						12.4		-36.2
	33	1355	13/150		135	3mm	HH	6.2	Clutter	-31.7
	34							4.5		-29.1
	35		14/150					3.0		-26.5
	36							9.3		-33.2
	37	1409		1.5				12.4		-33.6
	40	1423	16/135		135	X	HH	6.2	Clutter	-18.0
	41							9.3		-18.7
	42							12.4		-20.3
	43	1433		2.0				18.6		-28.4
8 Aug	7	1547	12.5/180	2.0	095	3mm	HH	6.0	Clutter	-36.5
	8							3.0		-40.0
	9							4.5		-34.9
	10							9.0		-37.2
	11	1606			140	3mm	HH	9.0	Clutter	-36.8
	12							6.2		-34.6
	13							4.5		-38.3
	14	1515						3.0		-35.8
	17	1628			090			6.2		-35.3

TABLE VII (Continued)

Summary of Cross Section and σ° Data

Date	Run	Time	Wind Sp/Dir	h_{av}	Look	Band	Pol	Range	Target	σ or σ°
8 Aug	18	1635			140	X	HH	12.4	Clutter	-30.8
	19							9.3		-28.7
	20	1642						6.2		-24.0
	28	1656	8/225	2	095	3mm	VV	9.0	Clutter	-37.9
	29							6.2		-40.9
	30	1705						4.5		-45.8
9 Aug	8	1206	9.5/150	1.5	140	3mm	VV	6.2	Clutter	-40.8
	9	1226					HH	6.2		-33.8
	10	1232					HH	3.0		-34.2
	11	1252					VV	3.0		-37.6
	12	1300	10/150		140	X	VV	6.2	Clutter	-27.8
	13	1308					HH	6.2		-27.6
	15	1406	12.5/150		140	3mm	VV	3.1	Clutter	-37.2
	16	1412					VV	6.2		-36.7
	17	1432					HH	6.2		-30.3
	18	1437					HH	3.1		-28.0
	19	1512		2.0	140	X	HH	6.2	Clutter	-23.0
	20	1522					VV	6.2		-25.5
10 Aug	2	0955	<4	0.5	130	3mm	HH	15.0	Drum buoy	-12.5

TABLE VII (Continued)

Summary of Cross Section and σ° Data

Date	Run	Time	Wind Sp/Dir	h_{av}	Look	Band	Pol	Range	Target	σ' or σ°
	10	1022			090	3mm	HH	74.0	Merchant Ship	+16.0
	11	1026			135			12.5	15' Outboard	+ 1.6
10 Aug	12	1031			135	3mm	HH	11.9	25' Fishing	+14.7
	13				135			12.1	4' Spar Buoy	- 1.5
	14				145			12.1	Drum Buoy	-14.6
	15				135			15.4	20' Fishing	+12.8
	16							19	20' Sailboat	+ 1.4
	17	1059						17	20' Sailboat	+ 5.8
	18	1105			140	X	VV	15.4	Barge	+23.4
	19							15	Clutter	-56.1
	21	1158			180	3mm	HH	4.2	Swimmer with Mask	-14.8
	2	1204						4.2	Swimmer without mask	-13.8
11 Aug	7	0933	<4	0.6	090	3mm	HH	4.0	6" Al. Sphere	-12.2
	8								12" Al. Sphere	+ 0.7
	9								AN/SSQ-41 Sono	-6.7
	10								Clutter	In noise
	11								AN/SSQ-50 Sono	- 1.4
	12								AN/SSQ-49 Sono	- 0.1
	13	1021							Clutter	In noise
	14	1059			110	3mm	HH	5.6	6" Al. Sphere	-18.4
	15								12" Al. Sphere	- 5.9
	16								AN/ASQ-41 Sono	- 7.8

TABLE VII (Continued)

Summary of Cross Section and $\sigma°$ Data

Date	Run	Time	Wind Sp/Dir	h_{av}	Look	Band	Pol	Range	Target	σ' or $\sigma°$
	17								Clutter	In noise
	18								AN/SSQ-50 Sono	- 8.3
	19								AN/SSQ-50 Sono	- 5.1
	20								Clutter	-40.8
	21	1242							Swimmer	-13.0
	22	1320			110	3mm	HH	9.0	12" Al. Sphere	-11.6
	23	1348					VV		AN/SSQ-41 Sono	-19.1
12 Aug	1	1006	<4		135	3mm	VV	5.6	10' Fiberglass Boat	- 7.5
	9	1045			135	X	VV	8.4	10' Fiberglass Boat	- 0.8
	10	1048						7.5	Clutter	-60.0
13 Aug	1	0918	<4	1.0	150	X	VV	5.6	10' Fiberglass	- 9.2
	2	0922						5.0	Clutter	-41.5
	5	0943			150	3mm	VV	5.6	10' Fiberglass	+ 2.6
	6	0951						5.2	Clutter	-45.7
	13	1416			150	X	VV	7.2	12' Al. Sphere	-21.8
	14	1425						7.0	Clutter	-45.7
	17	1448	6/15– 7.7							
	18	1457						7.0	Clutter	-35.3

TABLE VII (Continued)

Summary of Cross Section and σ° Data

Date	Run	Time	Wind Sp/Dir	h_{av}	Look	Band	Pol	Range	Target	σ' or σ°
	25	1529			150	X	VV	7.0	AN/SSQ-49 Sono	-17.8
	26	1550						6.7		-36.0
	29	1607	6/150	1.5	150	3mm	VV	7.0	AN/SSQ-50 Sono	- 9.2
	30	1610						6.7	Clutter	-35.9
13 Aug	33	1633			150	X	VV	7.0	AN/SSQ-50 Sono	-19.3
	34	1641						7.2	Clutter	-38.0
17 Aug	3	1109	11/090	1.5	090	3mm	VV	6.2	Clutter	-40.9
	4				110					-40.7
	5				100					-41.1
	6				120					-41.0
	7				090					-40.8
	8				080					-40.8
	9				070					-40.6
	10	1138			060					-39.9
18 Aug	3	0930	10.5/090	2.5	090	3mm	VV	4.55	Clutter	-35.2
	4	0940						4.35	AN/SSQ-41 Buoy	-13.4
	5	1010						4.2	Clutter	-36.2
	6	1020						4.4	12" Al. Sphere	-12.4
	7	1103	7/090		090	3mm	HH	4.4	12" Al. Sphere	-10.0
	8	1105						4.2	Clutter	-32.2

TABLE VII (Continued)

Summary of Cross Section and σ° Data

Date	Run	Time	Wind Sp/Dir	h_{av}	Look	Band	Pol	Range	Target	σ' or σ°
19 Aug	1	0837	5.5/090	1.0	090	X	HH	10.0	Clutter	-35.8
	2							14.4		-44.8
	3							18.6		-45.9
	5				090	X	VV	8.0	Clutter	-32.6
	6							14.4		-40.0
	7	0902						18.6		-44.4
	16	1130	6/090		090	3mm	VV	3.2	Clutter	-37.6
	20	1329	7/090		090	3mm	VV	3.2	Clutter	-32.6
	21	1345					HH	3.2		-30.6

Multiple Radar

Date______ Recorder______ Operators______

day mo. yr.

Radar A______ h_{av} =

Radar B______

Radar C______

Run	Begin	Wind	Range	Az.	Target	Channel Q_1	Q_2	Q_3	Q_4	

Page No.______ From______ To______

Figure 28. Manual-entry data form

UNCLASSIFIED

Security Classification

DOCUMENT CONTROL DATA - R & D

(Security classification of title, body of abstract and indexing annotation must be entered when the overall report is classified)

1. ORIGINATING ACTIVITY (Corporate author) Engineering Experiment Station Georgia Institute of Technology Atlanta, Ga. 30332	2a. REPORT SECURITY CLASSIFICATION Unclassified 2b. GROUP

3. REPORT TITLE

Low-Angle Radar Sea Return at 3-mm Wavelength

4. DESCRIPTIVE NOTES (Type of report and inclusive dates)

Final Technical Report

5. AUTHOR(S) (First name, middle initial, last name)

Wayne K. Rivers

6. REPORT DATE	7a. TOTAL NO. OF PAGES	7b. NO. OF REFS
15 November 1970	vii + 74	18

8a. CONTRACT OR GRANT NO. N62269-70-C-0489 b. PROJECT NO. c. d.	9a. ORIGINATOR'S REPORT NUMBER(S) 9b. OTHER REPORT NO(S) (Any other numbers that may be assigned this report)

10. DISTRIBUTION STATEMENT

None

11. SUPPLEMENTARY NOTES	12. SPONSORING MILITARY ACTIVITY
Georgia Tech Project A-1268	Naval Air Development Center Johnsville, Pa. 18974

13. ABSTRACT

Measurements of the radar return from the sea and targets on the sea ~~have been~~ made at incidence angles near grazing with a 3-millimeter radar, developed and operated by personnel of the Naval Air Development Center, ~~Johnsville,~~ Pa. The results show similarities in many respects to sea return at longer wavelengths, but they are strikingly different in a few instances. Notable are that the trend for cross section per unit area to increase with decreasing wavelength from 10 to 3 cm is not continued between 3 cm and 3 mm, and that the return for vertical polarization is substantially less than that for horizontal polarization for all conditions observed. Also included in the study are indications of angle, wind-speed, and boresight-wind-vector angle dependences of sea return.

DD FORM 1 NOV 65 1473 (PAGE 1)

UNCLASSIFIED

Security Classification

14 KEY WORDS	LINK A		LINK B		LINK C	
	ROLE	WT	ROLE	WT	ROLE	WT
Cross Section	2,7,8					
Wind-Speed	6					
Range	6					
Polarization	6					
Sea Clutter	7,8					
3-mm	9					
X-band	9					
Boats	9					
Sonobuoys	9					
Radar	10					